Cell Stem Cell

Article

Activation of HERV-K(HML-2) disrupts cortical patterning and neuronal differentiation by increasing NTRK3

Graphical abstract

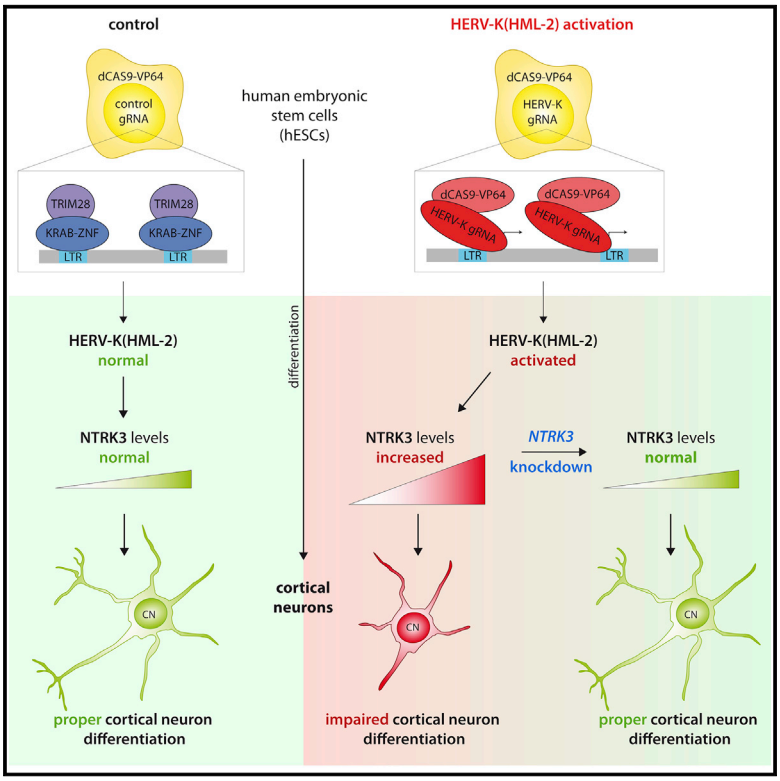

Authors

Vidya Padmanabhan Nair, Hengyuan Liu, Gabriele Ciceri, ..., Dmitrij Frishman, Lorenz Studer, Michelle Vincendeau

Correspondence

michelle.vincendeau@helmholtz-muenchen.de

In brief

Vincendeau and colleagues demonstrate that activation of the endogenous retrovirus group HERV-K(HML-2) negatively impacts cortical neuronal development by activating the classical developmental factor NTRK3. Intriguingly, while HERV-K(HML-2) activation impairs NTRK3-dependent cortical neurogenesis, NTRK3-independent dopaminergic neuronal differentiation is not affected.

Highlights

- Activation of HERV-K(HML-2) disrupts cortical neuron differentiation and function
- HERV-K(HML-2) activation induces NTRK3 expression
- Enhanced NTRK3 expression impairs cortical neuron differentiation
- Reducing NTRK3 levels in HERV-K(HML-2) activated cells restores differentiation

Padmanabhan Nair et al., 2021, Cell Stem Cell *28*, 1–16
September 2, 2021
https://doi.org/10.1016/j.stem.2021.04.009

CellPress

Cell Stem Cell

CellPress

Article

Activation of HERV-K(HML-2) disrupts cortical patterning and neuronal differentiation by increasing NTRK3

Vidya Padmanabhan Nair,[1] Hengyuan Liu,[2] Gabriele Ciceri,[3] Johannes Jungverdorben,[3] Goar Frishman,[4] Jason Tchieu,[3,7] Gustav Y. Cederquist,[3] Ina Rothenaigner,[5] Kenji Schorpp,[5] Lena Klepper,[1] Ryan M. Walsh,[3] Tae Wan Kim,[3] Daniela Cornacchia,[3] Andreas Ruepp,[4] Jens Mayer,[6] Kamyar Hadian,[5] Dmitrij Frishman,[2] Lorenz Studer,[3] and Michelle Vincendeau[1,3,8,*]

[1]Institute of Virology, Helmholtz Zentrum München, Neuherberg, Germany
[2]Department of Genome-Oriented Bioinformatics, Technical University Munich, Munich, Germany
[3]Developmental Biology and Center for Stem Cell Biology, Memorial Sloan Kettering Cancer Center, New York, NY, USA
[4]Institute of Experimental Genetics, Helmholtz Zentrum München, Neuherberg, Germany
[5]Assay Development and Screening Platform, Helmholtz Zentrum München, Neuherberg, Germany
[6]Institute of Human Genetics, University of Saarland, Homburg, Germany
[7]Present address: UC Department of Pediatrics, Division of Developmental Biology, Cincinnati Children's Hospital Medical, Cincinnati, OH, USA
[8]Lead contact
*Correspondence: michelle.vincendeau@helmholtz-muenchen.de
https://doi.org/10.1016/j.stem.2021.04.009

SUMMARY

The biological function and disease association of human endogenous retroviruses (HERVs) are largely elusive. HERV-K(HML-2) has been associated with neurotoxicity, but there is no clear understanding of its role or mechanistic basis. We addressed the physiological functions of HERV-K(HML-2) in neuronal differentiation using CRISPR engineering to activate or repress its expression levels in a human-pluripotent-stem-cell-based system. We found that elevated HERV-K(HML-2) transcription is detrimental for the development and function of cortical neurons. These effects are cell-type-specific, as dopaminergic neurons are unaffected. Moreover, high HERV-K(HML-2) transcription alters cortical layer formation in forebrain organoids. HERV-K(HML-2) transcriptional activation leads to hyperactivation of NTRK3 expression and other neurodegeneration-related genes. Direct activation of NTRK3 phenotypically resembles HERV-K(HML-2) induction, and reducing NTRK3 levels in context of HERV-K(HML-2) induction restores cortical neuron differentiation. Hence, these findings unravel a cell-type-specific role for HERV-K(HML-2) in cortical neuron development.

INTRODUCTION

Approximately 45% of the human genome consists of DNA transposons and retrotransposons, including human endogenous retroviruses (HERVs) (van de Lagemaat et al., 2003). HERVs belong to the long terminal repeat (LTR) family of retrotransposons and comprise 8% of the human genome (Mager and Medstrand, 2003). Several groups of phylogenetically distinct HERVs are transcriptionally active, and some HERV groups code for retroviral proteins/peptides (Bannert and Kurth, 2004; Chan et al., 2019; Ovejero et al., 2020; Zhang et al., 2019). Also, the human genome contains up to 500,000 copies of solitary LTRs (Buzdin et al., 2006), many of which are transcriptionally active. At least half of the LTRs investigated show promoter activity and therefore contribute to the cellular transcriptome (Buzdin et al., 2006; Faulkner et al., 2009; Schmitt et al., 2013). In line with this, many recent studies provided compelling evidence that HERVs critically influence biological processes, including placenta development, pluripotency of stem cells, or viability and migration of teratocarcinoma cells (Chan et al., 2019; Ellinghaus et al., 2008; Guffanti et al., 2019; Prudhomme et al., 2004; Seifarth et al., 2005; van de Lagemaat et al., 2003; Vincendeau et al., 2015; Wang et al., 2014). Moreover, HERV-derived enhancers can influence gene regulation and thus affect important biological processes, including early embryogenesis (Fuentes et al., 2018) or innate immunity (Chuong et al., 2016). Consequently, HERVs are now regarded as an important force in genome evolution and adaptation of an organism to altered environmental conditions. An important example of the suspected contributions of HERV to disease outcomes is the increased expression of HERV-K in schizophrenia, bipolar disorders (Frank et al., 2005), and amyotrophic lateral sclerosis (ALS) (Li et al., 2015), although in the case of ALS, increased HERV-K expression is controversial (Garson et al., 2019a, 2019b; Mayer et al., 2018; Prudencio et al., 2017).

HERV groups can consist of several hundreds to thousands of sequences, making it challenging to perform functional studies and identify their impact on biological processes. Recent studies investigated the regulation of retrotransposons, including HERVs, by manipulating their cellular regulators such as KAP1

Please cite this article in press as: Padmanabhan Nair et al., Activation of HERV-K(HML-2) disrupts cortical patterning and neuronal differentiation by increasing NTRK3, Cell Stem Cell (2021), https://doi.org/10.1016/j.stem.2021.04.009

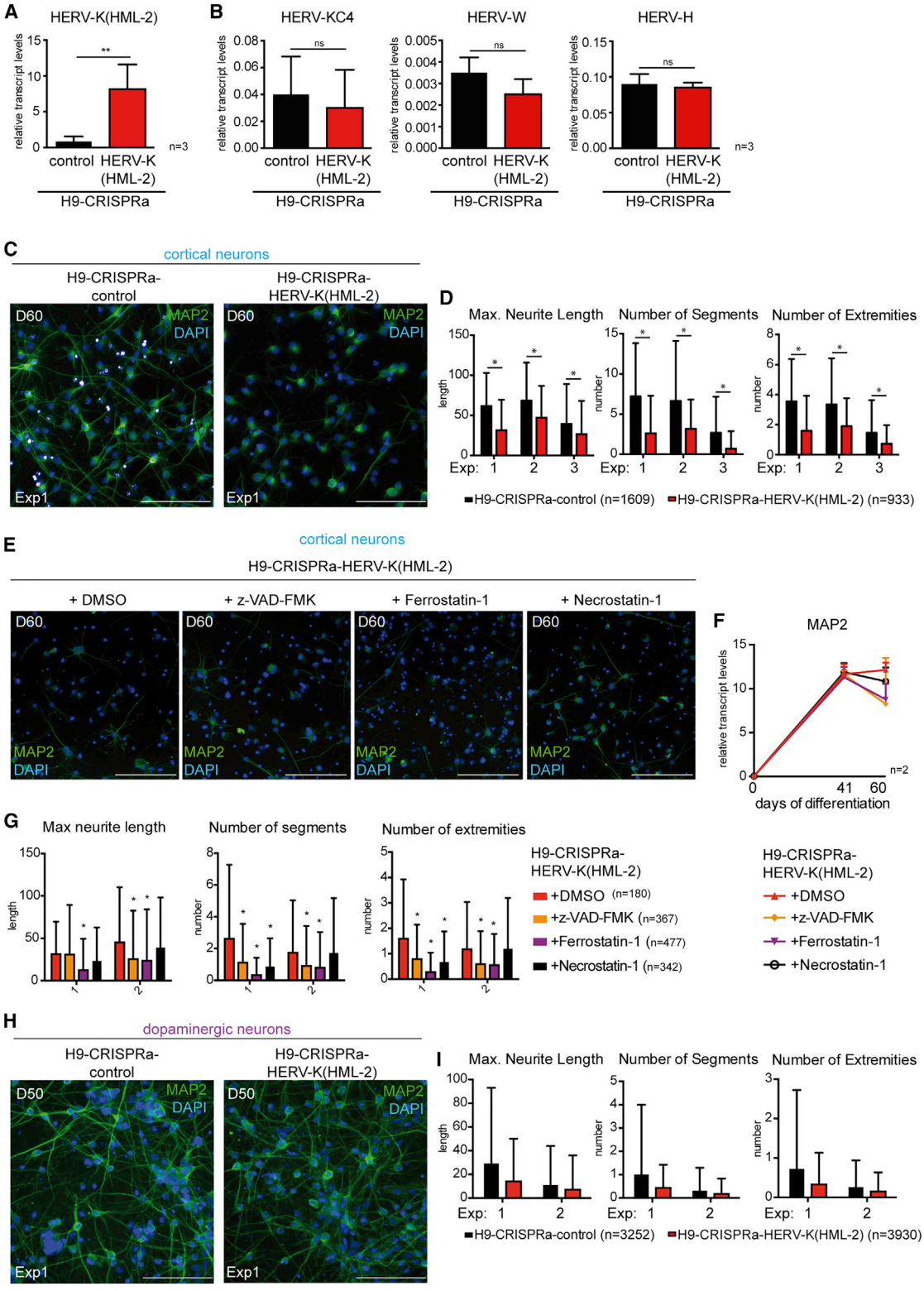

Figure 1. HERV-K(HML-2) activation reduces MAP2 expression and changes the morphology of cortical neurons

(A) HERV-K(HML-2) transcript levels upon CRISPRa treatment were quantified by qRT-PCR. n = 3 biological replicates.

(B) Expression of HERV groups HERV-KC4, HERV-W, and HERV-H in H9-CRISPRa-HERV-K(HML-2) cells was analyzed by qRT-PCR. n = 3 biological replicates.

(C) H9-CRISPRa-HERV-K(HML-2) cells and control cells were differentiated into cortical neurons. MAP2 expression was analyzed by immunofluorescence at day 60. One out of three independent differentiations is shown. Scale bars, 100 μm. The white dots come from oversaturated DAPI staining of dead neurons.

(legend continued on next page)

Please cite this article in press as: Padmanabhan Nair et al., Activation of HERV-K(HML-2) disrupts cortical patterning and neuronal differentiation by increasing NTRK3, Cell Stem Cell (2021), https://doi.org/10.1016/j.stem.2021.04.009

in human stem cells. Deletion of KAP1 during murine brain development resulted in multifaceted behavioral changes (Fasching et al., 2015; Jakobsson et al., 2008). Moreover, loss of KAP1 in mouse neural progenitor cells (NPCs), upon CRISPR-mediated KAP1 knockout, resulted in an increase in ERV expression, whereas KAP1 deletion in adult mouse neurons did not alter ERV expression (Jönsson et al., 2021). However, as KAP1 regulates the dynamic organization of chromatin structures and thereby almost all transposable elements (Ecco et al., 2016; Helleboid et al., 2019), it is difficult to discriminate between changes in gene regulatory networks caused by HERVs or other retrotransposable elements, such as SVA elements (SINE-VNTR-Alus), which share specific regions of specific HERV groups (Hancks and Kazazian, 2010).

In this report, we undertook a CRISPR-based approach to directly modulate the activity of several distinct HERV-K(HML2) promoters in order to elucidate the function of this HERV group on neuronal differentiation.

RESULTS

HERV-K(HML-2) transcriptional activation impairs cortical neuronal differentiation

To better understand the impact of HERV-K(HML-2) on neuronal differentiation processes, we used the CRISPR activation (CRISPRa) method to activate LTR promoters of HERV-K(HML-2) proviruses and solitary LTRs in human embryonic stem cells (hESCs). We generated a H9-dCas9-VP64 cell line and confirmed genome integration and expression of dCas9 by analyzing genomic DNA and mRNA levels (Figures S1A and S1B). For the specific modulation of HERV-K(HML-2) LTRs, we designed gRNA sequences binding within HERV-K(HML-2) LTRs. We analyzed sequences of ~600 HERV-K(HML-2) LTRs to identify little variable sequence portions for gRNA design in order to simultaneously modulate a large number of LTRs. We selected two gRNAs (gRNA3 and gRNA10; Figure S1G), representing ~70% of HERV-K(HML-2) LTRs, and transduced H9-dCas9-VP64 cells with these two gRNA constructs, thereby generating H9-CRISPRa-HERV-K(HML-2) cells. Using qRT-PCR, we verified elevated HERV-K(HML-2) mRNA levels by CRISPRa (Figure 1A). Also, immunofluorescence analyses using an antibody directed against HERV-K(HML-2) Gag confirmed HERV-K(HML-2) activation in H9-CRISPRa-HERV-K(HML-2) cells (Figure S1C). To investigate specificity of HERV-K(HML-2) gRNAs, we tested transcript levels of three other HERV groups (Figure 1B), specifically HERV-KC4, which is relatively closely related to HERV-K(HML-2), and HERV-W and HERV-H, which are both gammaretroviruses. Transcription of these groups was not affected in H9-CRISPRa-HERV-K(HML-2) cells (Figure 1B), corroborating specific activation of HERV-K(HML-2) transcription by the selected gRNAs. Notably, activation of HERV-K(HML-2) transcription did not affect levels of pluripotency markers NANOG or OCT-4 compared to control cells (Figure S1D).

To investigate whether HERV-K(HML-2) activation influences differentiation of hESCs into cortical neurons, we differentiated H9-CRISPRa-HERV-K(HML-2) and control cells into cortical neurons (Cederquist et al., 2019; Riessland et al., 2019). Day 60 cortical neurons were analyzed for neuronal induction and morphology using MAP2 immunofluorescence staining in three independent differentiations (Figures 1C and S1E). MAP2a/b isoforms are neuron-specific cytoskeletal proteins and specifically expressed in the perikarya and dendrites. Therefore, MAP2 staining is a suitable marker for neuronal cells and investigating morphological (cytoskeletal) changes. Interestingly, HERV-K(HML-2) activated cortical neurons exhibited a drastic reduction in MAP2 staining (Figures 1C and S1E) compared to control cells. In addition, we noticed changes in neuronal morphology upon HERV-K(HML-2) transcriptional activation. To further address this, we used high-content image analysis to quantify morphological changes in 933 cells, revealing reduced neurite length as well as decreased numbers of segments and extremities in HERV-K(HML-2) activated cortical neurons (Figure 1D). Time-course analysis of *MAP2* expression at several steps of differentiation confirmed reduced *MAP2* mRNA levels in HERV-K(HML-2) activated cells throughout cortical differentiation (Figure S1F). To exclude off-target effects by the CRISPR technology and gRNA3, which also locates in various subtypes of SVA elements (Figure S1G), although with a suboptimal PAM sequence (AAG in SVAs with a <10% SpCas9 recognition rate; Kleinstiver et al., 2015; Tang et al., 2019), we used two additional gRNAs (gRNA 6 and 11) targeting other regions of the HERV-K(HML-2) LTR (Figure S1G). Likewise, this gRNA combination resulted in transcriptional activation of *HERV-K(HML-2)* (Figure S1H) as well as drastic reduction of MAP2 levels in cortical neurons (Figures S1I and S1J) and morphological changes (Figure S1K). In addition, to rule out that the differentiation phenotype is not due to cell death, we performed cortical differentiations upon HERV-K(HML-2) activation until day 60 in the presence of an apoptosis inhibitor (z-VAD-FMK), a ferroptosis inhibitor (ferrostatin-1), or a necroptosis inhibitor (necrostatin-1). We analyzed *MAP2* expression levels during the course of differentiation and treatment (Figures 1E and 1F). Inhibiting cell death pathways for apoptosis, ferroptosis, or necroptosis did not

(D) Morphological analyses of cortical neurons upon HERV-K(HML-2) activation. Three biological replicates were quantified each.
(E) H9-CRISPRa-HERV-K(HML-2) cells and control cells were differentiated into cortical neurons while treated with cell death inhibitors. MAP2 expression was analyzed by immunofluorescence at day 60. One out of two independent differentiations is shown. Scale bars, 100 μm.
(F) MAP2 transcript levels were analyzed by qRT-PCR. n = 2 biological replicates.
(G) Morphological analysis of cortical neurons upon HERV-K(HML-2) activation and cell death inhibition. Two biological replicates were quantified.
(H) HERV-K(HML-2) activated cells were differentiated into dopaminergic neurons. MAP2 expression was analyzed by immunofluorescence at day 50. One out of three independent differentiations is shown. Scale bars, 100 μm.
(I) Morphological analyses of dopaminergic neurons upon HERV-K(HML-2) activation. Two biological replicates were quantified.
(A and B) Values represent mean ± SD; unpaired two-tailed Student's t test (**$p < 0.01$, ns = non significant).
(G and I) Values represent mean ± SD; multiple t test using the Holm-Sidak method (*$p < 0.05$).

Please cite this article in press as: Padmanabhan Nair et al., Activation of HERV-K(HML-2) disrupts cortical patterning and neuronal differentiation by increasing NTRK3, Cell Stem Cell (2021), https://doi.org/10.1016/j.stem.2021.04.009

change *MAP2* levels (Figures 1E–1F) and did not revert morphological changes in cortical neurons with activated HERV-K(HML-2) (Figure 1G). Also, no changes in caspase-3 expression were observed in pluripotent stem cells or cortical neurons generated from HERV-K(HML-2) activated and control cells (Figure S1L). Overall, these data show that the phenotype observed upon HERV-K(HML-2) activation is not based on off-target or toxic effects.

To test whether the effects observed upon HERV-K(HML-2) activation are specific to cortical neurons, we performed directed differentiation of H9-CRISPRa-HERV-K(HML-2) and control cells into dopaminergic neurons (Figures 1H and S1M) (Kim et al., 2021; Riessland et al., 2019). At day 50 of dopaminergic differentiation, we stained dopaminergic neurons from HERV-K(HML-2) activated cells as well as control cells for MAP2. Intriguingly, dopaminergic neurons showed no decreased MAP2 expression (Figures 1H and S1M) upon HERV-K(HML-2) activation. We investigated 3,930 HERV-K(HML-2) activated dopaminergic neurons for changes in morphology using high-content image analysis (Figure 1I). We observed no changes in neurite length or numbers of segments and extremities upon HERV-K(HML-2) activation (Figure 1I). Importantly, we checked HERV-K(HML-2) expression in cortical and dopaminergic neurons and demonstrated that HERV-K(HML-2) is activated to the same extent in cortical neurons (day 60) and dopaminergic neurons (day 50), thereby ruling out that lack of phenotype in dopaminergic neurons is due to lesser activation of HERV-K(HML-2) (Figure S1N). These results show that the reduced *MAP2* expression observed in cortical neurons may be specific to distinct types of neurons and not a ubiquitous phenomenon.

HERV-K(HML-2) transcriptional activation during cortical neuronal differentiation compromises cortical neuron functionality

Next, we investigated functionality of differentiated cortical as well as dopaminergic neurons by examining synapsin I expression levels (Figures 2A, 2C, S2A, and S2C). Immunofluorescence for synapsin I at day 60 showed a reduction of synapsin I staining in HERV-K(HML-2) activated cortical neurons in three independent cortical neuronal differentiations (Figures 2A and S2A). We quantified 419 Synapsin-I-expressing cells for spot area, spot intensity, and spot number using high-content image analysis (Figure 2B). While there is synapsin I protein observed also in the cytoplasm of neurons, functionally relevant synapsin I (presynaptic marker) localizes to the synapse. Thus, we quantified putative synaptic punctae. Whereas spot area was not affected, synapsin I spot number was evidently decreased in HERV-K(HML-2) activated cortical neurons (Figure 2B). Moreover, we confirmed decrease of *SYNAPSIN I* transcript levels in HERV-K(HML-2) activated cortical neurons starting at approximately day 20 (Figure S2B). As expected, dopaminergic neurons showed no decreased *SYNAPSIN I* expression (Figures 2C and S2C) upon HERV-K(HML-2) activation. Also, quantification of 1,618 HERV-K(HML-2) activated dopaminergic neurons confirmed no changes of spot area or spot number (Figure 2D). Overall, these results suggest decreased neuronal functionality in HERV-K(HML-2) activated cortical neurons. To further confirm loss of neuronal functionality in HERV-K(HML-2) activated cortical neurons, we carried out calcium imaging at day 45 of cortical neuronal differentiation (Figures 2E–2F). Cells were treated with calcium dye Fura-2 and imaged for calcium levels upon stimulation. A glutamate pulse generated a calcium response, which results in a calcium peak (Tchieu et al., 2019). Indeed, we detected increased Ca^{2+} levels in control neurons transduced with control gRNAs, but the calcium response was weaker in cortical neurons with activated HERV-K(HML-2) (Figure 2E). We quantified the strength of the calcium response at the time point 20 min (time point of main peak) and observed a significantly reduced calcium response in HERV-K(HML-2) activated cortical neurons compared to the control (Figure 2F). Thus, activation of HERV-K(HML-2) impairs functionality of differentiated cortical neurons.

We next addressed whether transcription of HERV-K(HML-2) is necessary to promote or enhance cortical neuronal differentiation. To do so, we targeted the KRAB repressor to HERV-K(HML-2) by fusing it to dCas9 using a similar strategy as above for CRISPRa. We achieved reduction of HERV-K(HML-2) expression by ~60% in non-differentiated hESCs stably expressing the CRISPR inhibition system (Figure S2D**)**. We performed directed differentiation of these cells into cortical neurons to examine the phenotype upon HERV-K(HML-2) repression. Transcriptional repression of HERV-K(HML-2) during cortical differentiation had no impact on MAP2 expression (Figure S2E). Moreover, we did not observe changes in neuronal morphology, such as neurite length or number of segments or extremities (Figure S2F), using high-content image analysis of 1,618 HERV-K(HML-2) activated cells. Together, our results demonstrate that transcriptional activation of HERV-K(HML-2) LTRs negatively affects functionality of cortical neurons, whereas dopaminergic neurons are unaffected.

HERV-K(HML-2) activation leads to defective forebrain organoid patterning

To further investigate effects of HERV-K(HML-2) transcriptional activation in a physiological 3D context of brain development, we generated forebrain organoids using H9-CRISPRa-HERV-K(HML-2) or control cells (Figure 3A). At time points day 20 and day 60, we confirmed increased expression of HERV-K(HML-2) in organoids generated from H9-CRISPRa-HERV-K(HML-2) cells compared to control cells (Figure S3A). Interestingly, organoids with activated HERV-K(HML-2) expression exhibited a significantly reduced size at day 60 compared to control organoids (Figure 3B).

We performed caspase-3 (Figure S3B) and KI67 (Figure S3C) staining to control for differences in apoptosis and proliferation in control as well as HERV-K(HML-2) activated organoids at day 60. No difference in caspase-3 (Figure S3B) or KI67 (Figure S3C) staining between control and HERV-K(HML-2) activated organoids could be observed. Thus, we excluded toxic or cell proliferation effects upon HERV-K(HML-2) activation. Next, we investigated the influence of HERV-K(HML-2) activation on laminar brain patterning. At day 60, organoids with transcriptionally active HERV-K(HML-2) resulted in a diffuse and unorganized distribution of $CTIP2^+$ (Figures 3C and S3D) as well as $TBR1^+$ (Figures 3F and S3E) neurons. In contrast, $CTIP2^+$ and $TBR1^+$ neurons were structured in the control organoids generating a sharp CTIP2 (Figures 3C and S3D) as well as TBR1 layer (Figures 3F and S3E). However, HERV-K(HML-2) activation did not affect the well-defined ventricular-zone-like structure in forebrain

Please cite this article in press as: Padmanabhan Nair et al., Activation of HERV-K(HML-2) disrupts cortical patterning and neuronal differentiation by increasing NTRK3, Cell Stem Cell (2021), https://doi.org/10.1016/j.stem.2021.04.009

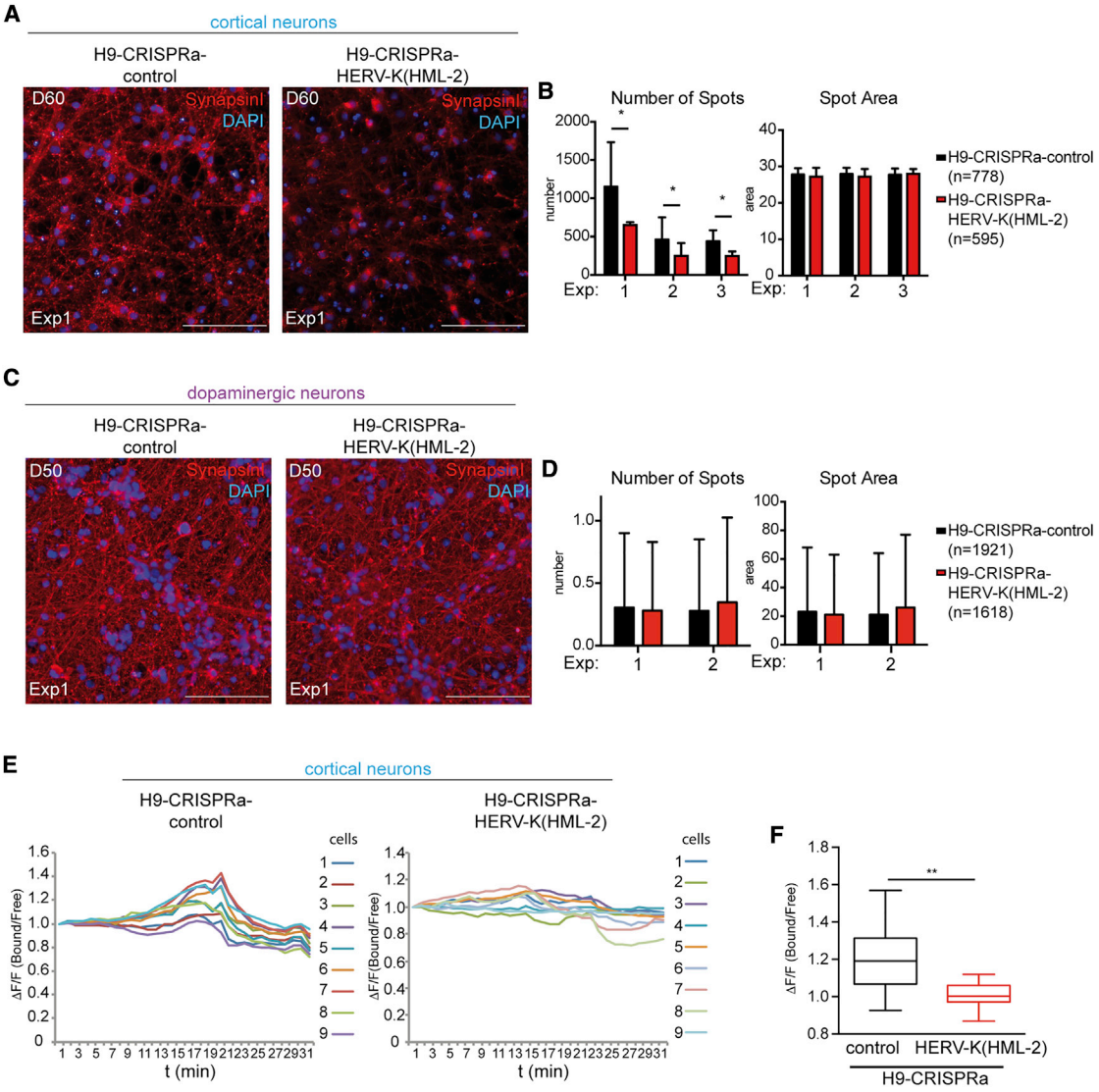

Figure 2. HERV-K(HML-2) activation reduces functionality of cortical neurons

(A) Synapsin I levels were examined by immunofluorescence in HERV-K(HML-2) activated and control cortical neurons at day 60. One out of three biological replicates is shown.

(B) Synapsin I spot number and area were quantified by high-content image analysis in HERV-K(HML-2) activated and control cortical neurons. Three biological replicates were quantified.

(C) Synapsin I levels were examined by immunofluorescence in HERV-K(HML-2) activated and control dopaminergic neurons at day 50. One out of two biological replicates is shown.

(D) Synapsin I spot number and area were quantified by high-content image analysis in HERV-K(HML-2) activated and control dopaminergic neurons. Two biological replicates were quantified.

(E) Calcium imaging was carried out at day 45 of differentiation in HERV-K(HML-2) activated and control cortical neurons. n = 2 biological replicates.

(F) Calcium peaks were quantified at time point 20 min. Values represent mean ± SD; unpaired two-tailed Student's t test (**$p < 0.01$).

(B and D) Values represent mean ± SD; multiple t test using the Holm-Sidak method (*$p < 0.05$).

organoids, which contain PAX6 (Figures 3C and S3D) or SOX2 (Figures 3F and S3E) neural progenitor cells. The distribution of CTIP2$^+$, TBR1$^+$, PAX6$^+$, and SOX2$^+$ cells was further quantified by dividing the developing cortex into five equal bins, as described previously (Buchsbaum et al., 2020), with bin 1 corresponding to ventricular zone, bins 2 and 3 corresponding to subventricular zone, and bins 4 and 5 corresponding to cortical plate of the cortex (Figures 3D, 3E, 3G, and 3H). Upon HERV-K(HML-2) activation, significantly more CTIP2$^+$ cells localized in bins 3 and 4 and fewer cells localized in bin 5 compared to control cells (Figure 3D). The distribution of PAX6$^+$ cells was not significantly affected upon HERV-K(HML-2) activation (Figure 3E). In the case of TBR1, more TBR1$^+$ cells localized in bins 2 and 3, while the number of cells was significantly decreased in bin 5 upon HERV-K(HML-2) activation compared to control organoids (Figure 3G). The distribution of SOX2$^+$ cells was not changed upon

Please cite this article in press as: Padmanabhan Nair et al., Activation of HERV-K(HML-2) disrupts cortical patterning and neuronal differentiation by increasing NTRK3, Cell Stem Cell (2021), https://doi.org/10.1016/j.stem.2021.04.009

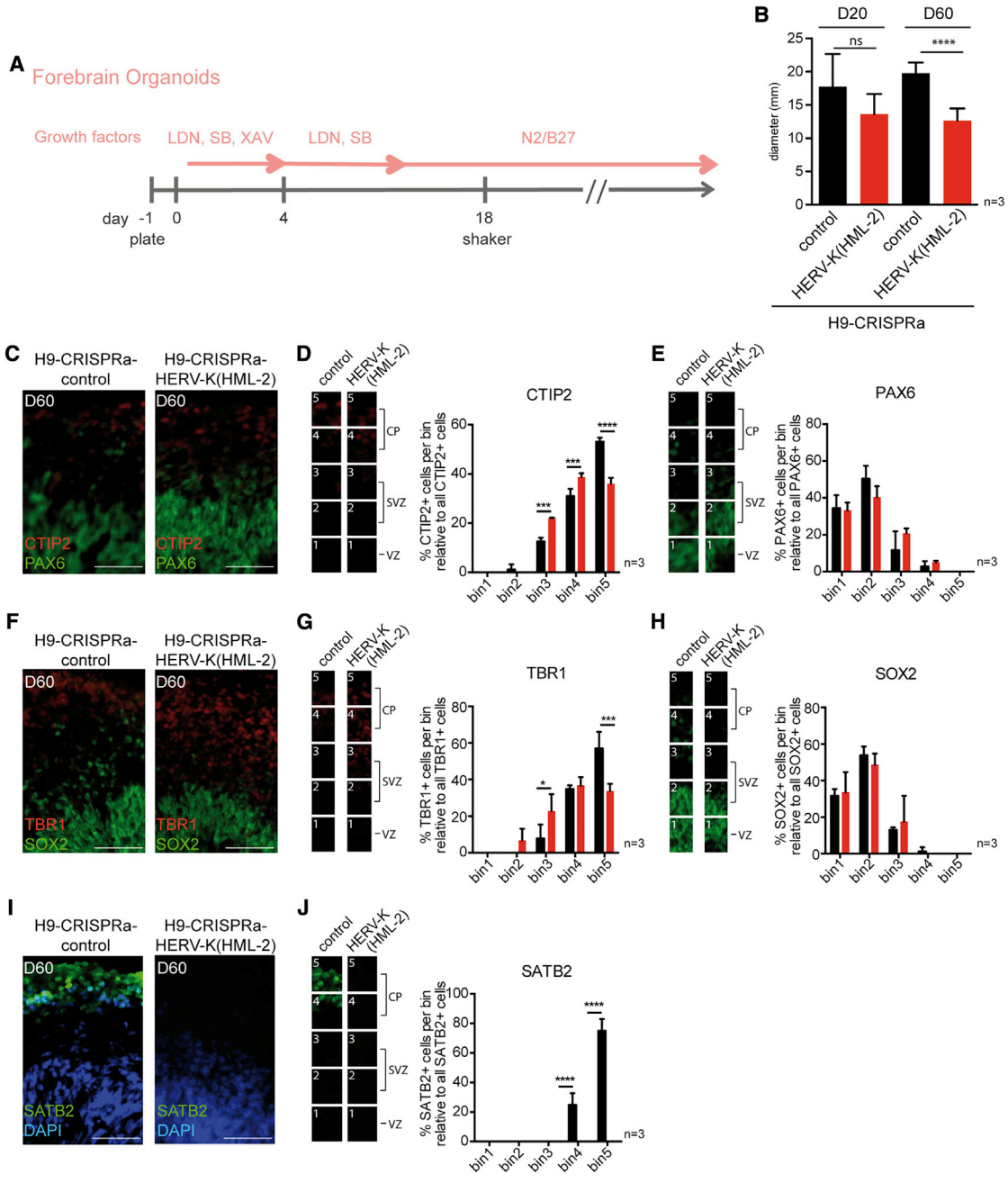

Figure 3. HERV-K(HML-2) activation changes patterning of CTIP2, TBR1, and SATB2 in forebrain organoids

(A) 3D forebrain organoids were generated as depicted.

(B) Size of forebrain organoids from HERV-K(HML-2) activated and control cells was measured at days 20 and 60 using ImageJ software. n = 3 biological replicates; unpaired two-tailed Student's t test (****$p < 0.0001$, ns = non significant).

(C, F, and I) Forebrain organoid sections from HERV-K(HML-2) activated and control cells of day 60 were stained for CTIP2/PAX6 (C), TBR1/SOX2 (F), and SATB2/DAPI (I). Scale bars, 50 μm.

(D, E, G, H, and J) Quantification of $CTIP2^+$, $PAX6^+$, $TBR1^+$, $SOX2^+$, and $SATB2^+$ cells using ImageJ analysis. n = 3 biological replicates; two-way ANOVA (*$p < 0.05$, ***$p < 0.001$, and ****$p < 0.0001$). CP, cortical plate; SVZ, subventricular zone; VZ, ventricular zone.

(C–J) Three independent biological replicates were performed, and three organoids per time point were sectioned, stained, and quantified.

HERV-K(HML-2) activation (Figure 3H). Next, we stained for SATB2 at day 60. A layer of late-born $SATB2^+$ neurons was visible in control organoids (Figures 3I and S3F), confirming a specification of multiple projection neuron subtypes. In contrast, organoids with HERV-K(HML-2) activation lacked the layer formed by $SATB2^+$ neurons (Figures 3I and S3F). We also quantified the $SATB2^+$ cells in HERV-K(HML-2) activated organoids and control organoids (Figure 3J). $SATB2^+$ cells could be observed in bins 4

Please cite this article in press as: Padmanabhan Nair et al., Activation of HERV-K(HML-2) disrupts cortical patterning and neuronal differentiation by increasing NTRK3, Cell Stem Cell (2021), https://doi.org/10.1016/j.stem.2021.04.009

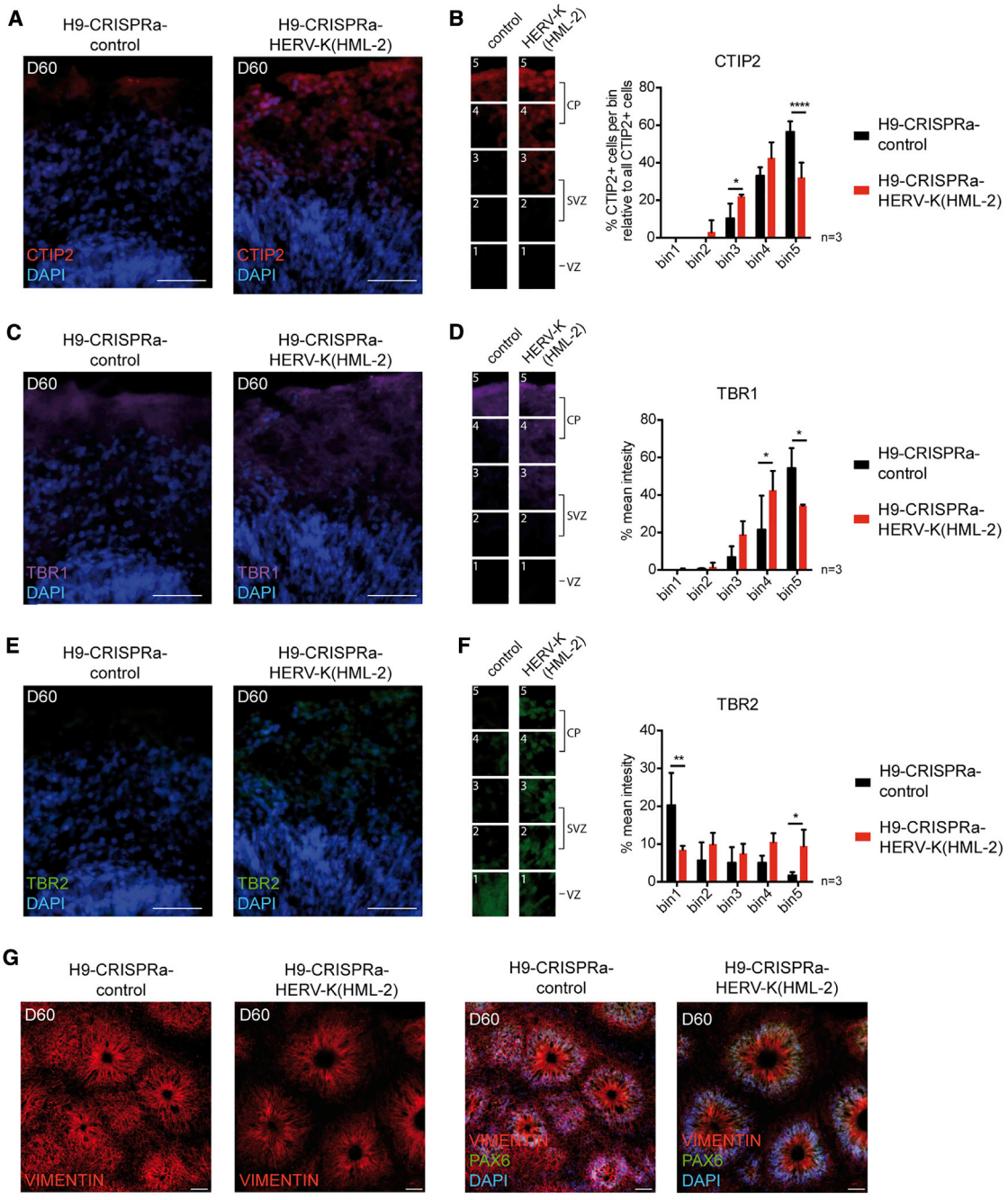

Figure 4. HERV-K(HML-2) activation changes patterning of TBR2 and vimentin in forebrain organoids

(A, C, and E) Sections of activated HERV-K(HML-2) forebrain organoids and control organoids were stained for CTIP2, TBR1, and TBR2. Scale bars, 50 μm.

(B, D, and F) CTIP2$^+$, TBR1$^+$, and TBR2$^+$ cells were quantified in activated HERV-K(HML-2) forebrain organoids and control organoids using ImageJ software. n = 3 biological replicates; two-way ANOVA(*p < 0.05, **p < 0.01, and ****p < 0.0001). CP, cortical plate; SVZ, subventricular zone; VZ, ventricular zone.

(G) Radial glia (RG) progenitors were stained for vimentin to analyze characteristic polarized morphology. Scale bars, 50 μm.

(A–F) Three independent biological replicates were performed, and three organoids per time point were sectioned, stained, and quantified.

and 5 of control organoids, whereas they were undetectable in any of the bins of HERV-K(HML-2) activated cells (Figure 3J).

We further triple stained day 60 forebrain organoids from control and HERV-K(HML-2) activated cells for CTIP2, TBR1, and TBR2 (Figures 4A, 4C, and 4E). In control forebrain organoid sections, we observed a dense population of neurons expressing CTIP2 and TBR1 and a more sparse population of TBR2$^+$ intermediate progenitor cells (IPCs) (Figures 4A, 4C, and 4E). In contrast, sections of transcriptionally activated HERV-K(HML-2) forebrain organoids showed less discrete layers of CTIP2$^+$, TBR1$^+$, and TBR2$^+$ cells (Figures 4A, 4C, and 4E). Quantification of the specific neuronal layers

Please cite this article in press as: Padmanabhan Nair et al., Activation of HERV-K(HML-2) disrupts cortical patterning and neuronal differentiation by increasing NTRK3, Cell Stem Cell (2021), https://doi.org/10.1016/j.stem.2021.04.009

(Figures 4B, 4D, and 4F) revealed more CTIP2$^+$ cells in bins 3 and 4 and fewer cells in bin 5 upon HERV-K(HML-2) activation compared to control organoids (Figure 4B). For TBR1, we quantified relative mean intensity, observing increased TBR1 intensity in bins 3 and 4 and decreased intensity in bin5 upon HERV-K(HML-2) activation compared to control organoids (Figure 4D). TBR2$^+$ cells were pushed more toward the pial side of organoids upon HERV-K(HML-2) activation, as they localized more in bin 5 and less in bin 1 compared to control organoids (Figure 4F). Thus, quantifications showed an unorganized distribution of CTIP2$^+$, TBR1$^+$, and TBR2$^+$ layers in HERV-K(HML-2) activated organoids compared to structured layers in the control (Figures 4B, 4D, and 4F). We also performed flow cytometry analysis of control and HERV-K(HML-2) activated organoids at day 60 as described previously (Buchsbaum et al., 2020), investigating CTIP2, TBR1, SATB2 and PAX6 expression (Figures S4A and S4B). We observed significant reduction in CTIP2$^+$, TBR1$^+$ and SATB2$^+$ cells in HERV-K(HML-2) activated organoids compared to control organoids (Figure S4A). Notably, we did not observe differences in PAX6 expression (Figure S4B). Besides, we stained for vimentin (Figure 4G), which is upregulated during epithelial to mesenchymal transition of neuroepithelia cells to radial glia (RG) cells. RG cells play key roles in neurogenesis, as they are considered as precursors of neuron generation in many regions of the developing brain. Overall stronger vimentin expression was observed in control forebrain organoids compared to HERV-K(HML-2) activated organoids. Control RG progenitors showed characteristic polarized morphology, with elongated polarized basal processes (Figure 4G). In contrast, activation of HERV-K(HML-2) resulted in short basal RG processes (Figure 4G). Additionally, we observed a decrease in the MAP2$^+$ neuronal layer in HERV-K(HML-2) activated forebrain organoids of day 60 compared to control forebrain organoids (Figure S4C), which was consistent with our observations of cortical neurons differentiated in monolayer. Together, these data demonstrate a disrupted forebrain organoid patterning upon HERV-K(HML-2) activation.

Induction of HERV-K(HML-2) activation at early stages of cortical neuronal differentiation negatively impacts cortical development

To decipher which step of cortical differentiation is impaired upon HERV-K(HML-2) transcriptional activation, we developed an inducible CRISPRa cell line that allowed us to induce HERV-K(HML-2) transcriptional activation at variable steps during differentiation. We used the generated cell line and induced HERV-K(HML-2) expression using doxycycline at three different stages during cortical differentiation: neuroectoderm (day 5), cortical progenitors (day 10), and immature neurons (day 21) (Figure 5A). A control-gRNA-expressing line induced at the same time points with doxycycline served as a control. At day 55 of cortical differentiation, we stained for MAP2 expression (Figure 5B). Cortical neurons with activated HERV-K(HML-2) at the stages of neuroectoderm (day 5) or cortical progenitors (day 10) showed drastically reduced MAP2 expression (Figure 5B) compared to control-gRNA-expressing cells. In contrast, when HERV-K(HML-2) was activated at the stage of immature neurons (day 21), no changes in MAP2 expression could be observed, which was comparable to control-gRNA-expressing cells (Figure 5B). Importantly, induction of HERV-K(HML-2) expression levels was always equally strong at the different time points during cortical differentiation, as evidenced by qRT-PCR (Figure S5A). We also monitored *MAP2* expression at days 41 and day 55 by qRT-PCR (Figures 5C–5F). Cells in which HERV-K(HML-2) was activated at day 5 or 10 showed reduced *MAP2* mRNA levels (Figures 5C and 5D), whereas *MAP2* mRNA levels were not affected in day-21-HERV-K(HML-2)-induced or control-gRNA-expressing cells (Figure 5E). Besides decreased MAP2 expression (protein and RNA levels), we also analyzed changes in neuronal morphology of cells in which HERV-K(HML-2) had been activated at day 5, 10, or 21. Quantification by high-content image analysis confirmed impaired neuronal morphology only for cells activated at days 5 and 10 (Figure 5F). These data suggest that HERV-K(HML-2) activation at earlier stages of neurogenesis affects neuronal development instead of the maintenance of neuronal identity or functionality.

HERV-K(HML-2) overexpression upregulates neuronal-development-related genes in cortical neurons

To investigate whether HERV-K(HML-2) activation affects gene expression, we induced cortical neuronal differentiation in H9-CRISPRa-HERV-K(HML-2) and control cells and performed total RNA sequencing (RNA-seq) at days 0, 10, 27, 41, and day 60. The overall similarity between HERV-K(HML-2) activated and control cells was assessed using principal-component analysis (PCA) of protein-coding genes, bidirectional promoter-derived long non-coding RNA (lncRNA), microRNA (miRNA), antisense RNA, and long intervening non-coding RNA (lincRNA). A significant expression shift upon HERV-K(HML-2) activation during the course of differentiation into cortical neurons was only detectable for protein-coding genes (Figures 6A and S6A). At day 0, HERV-K(HML-2) activated and control cells cluster together, attesting to a low degree of unspecific effects due to induced HERV-K(HML-2) levels. At later time points (days 27, 41, and 60), separate localization was seen for HERV-K(HML-2) activated cells and control cells, which became more pronounced as the cells progressed through differentiation. These findings imply that the observed transcriptome changes in protein-coding genes specifically derive from HERV-K(HML2) overexpression. We identified a total of 28 genes that showed the strongest upregulation over the course of differentiation into cortical neurons (top 25%; see STAR Methods) between HERV-K(HML-2) activated and control cells (Figure 6B; Table S1). According to Gene Ontology (GO) enrichment analysis, these 28 genes are significantly associated with biological processes related to neurobiology (Figure 6C) and the cellular component axon (Gene Ontology: GO:0030424), which shows a strong correlation to neurogenesis. Disease enrichment analysis also unequivocally points to several neurological diseases, including neurodegenerative and neuropsychiatric conditions such as mental disorder, bipolar disorder, and nervous system disease (Figure 6D). For a more in-depth analysis, we manually curated a network of interactions between the identified gene set and neurodegenerative diseases (Figure S6B) using the multifactorial database CIDeR (Lechner et al., 2012). Each interaction is documented by

Please cite this article in press as: Padmanabhan Nair et al., Activation of HERV-K(HML-2) disrupts cortical patterning and neuronal differentiation by increasing NTRK3, Cell Stem Cell (2021), https://doi.org/10.1016/j.stem.2021.04.009

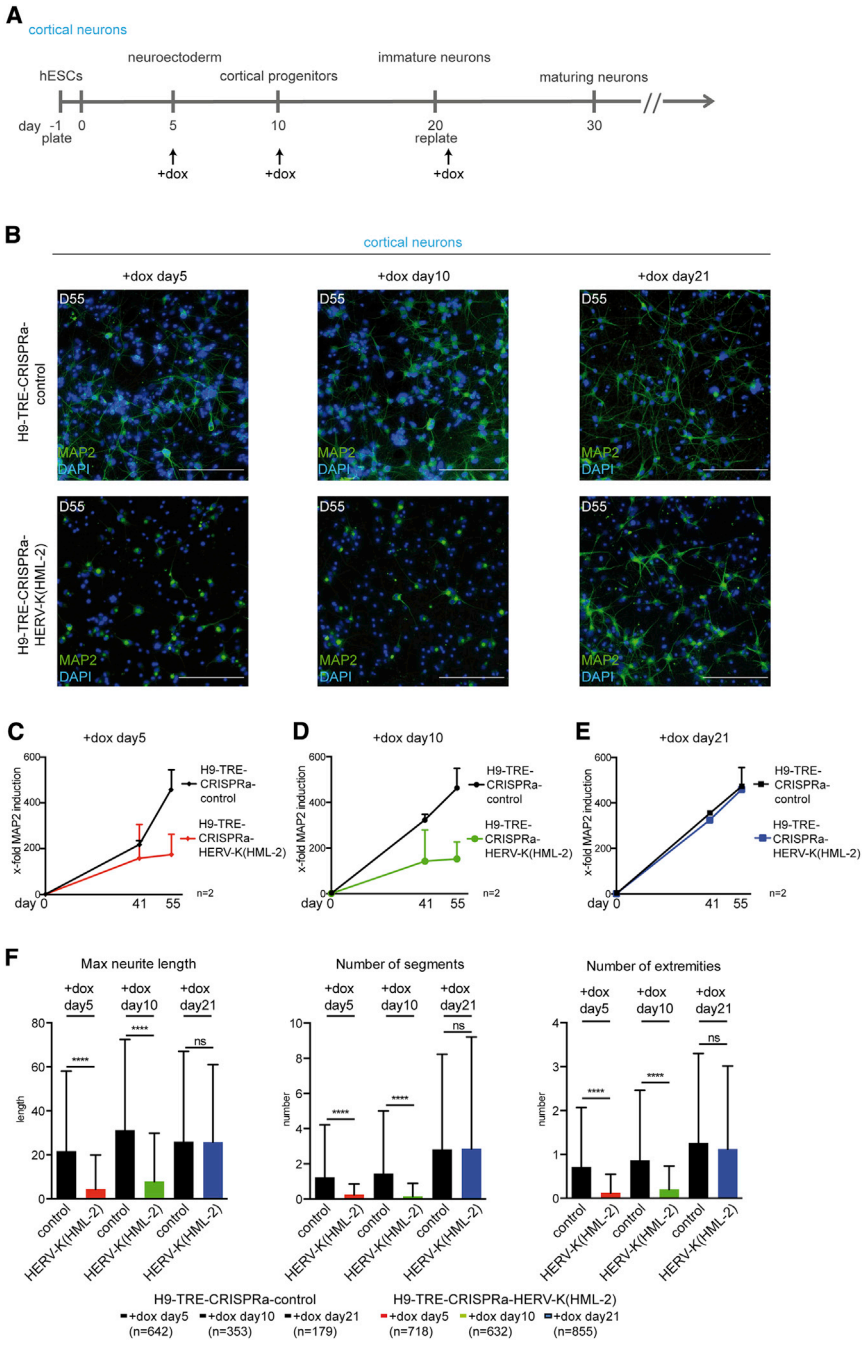

Figure 5. Induction of HERV-K(HML-2) activation at early stages of cortical neuronal differentiation impacts cortical development

(A) An inducible H9-TRE-CRISPRa-HERV-K(HML-2) and H9-TRE-CRISPRa-control cell lines were generated and induced by doxycycline at the following stages: neuroectoderm (day 5), cortical progenitors (day 10), and immature neurons (day 21).

(B) Cortical neurons with induced HERV-K(HML-2) activation at days 5, 10, and 21 were stained for MAP2 using immunofluorescence. Cortical neurons expressing a control gRNA upon doxycycline induction served as control. Scale bars, 100 μm.

(C) MAP2 repression was confirmed by qRT-PCR during cortical differentiation in TRE-HERV-K(HML-2) activated and TRE-control cells. n = 2 biological replicates.

(D) Morphological analysis of cortical neurons upon HERV-K(HML-2) induction. n = 2 biological replicates. Values represent mean ± SD; multiple t test using the Holm-Sidak method (****$p < 0.0001$, ns = non significant).

published experimental evidence. Interestingly, 25 out of the 28 identified upregulated genes are interconnected and directly or indirectly related to neurodegenerative diseases, processes, or phenotypes via SNP associations, expression, or regulation (Figure S6B). Among the identified upregulated genes (Table S1), four gene candidates were differentially expressed upon HERV-K(HML-2) activation. In particular, calsyntenin 2 (*CLSTN2*), chordin-like 1 (*CHRDL1*), EPH receptor A4 (*EPHA4*), and neurotrophic tyrosine receptor kinase 3 (*NTRK3*) were consistently highly upregulated at days 41 and 60 during cortical differentiation (Figures 6E, S6C, and S6D).

Activation of NTRK3 results in reduced MAP2 expression and changes in neuronal morphology

To investigate the underlying mechanism of how HERV-K(HML-2) activation affects cortical neuronal differentiation, we explored the impact of four genes confirmed by qRT-PCR (see Figure 6E) on cortical differentiation. We first developed H9 cells in which *CLSTN2*, *CHRDL1*, *EPHA4*, and *NTRK3* were activated using CRISPRa, achieving a 5- to 10-fold increase in respective mRNA levels (Figure 7A). We subjected each of the four cell lines to directed differentiation into cortical neurons. We examined expression of neuronal marker MAP2 in neurons at days 40 and 60 of cortical differentiation using immunofluorescence and qRT-PCR (Figures 7B, 7C, S7A, and S7B). Only in cortical neurons generated from H9 cells with *NTRK3* activation could we observe reduced MAP2 expression (Figures 7B, 7C, S7A, and S7B) and changes in neuronal morphology, such as reduced neurite length, number of segments, and number of extremities (Figures 7D and S7C). Activation of genes *CLSTN2*, *CHRDL1*, and *EPHA4* had minimal or no effect on MAP2 expression and neuronal morphology. Intriguingly, the phenotype observed upon *NTRK3* activation (Figures 7B and S7A) was almost identical to the phenotype upon HERV-K(HML-2) activation (Figures 1C, 1D, S1E, S1I, and S1K). Moreover, we evaluated whether *NTRK3* is also upregulated after HERV-K(HML-2) activation in dopaminergic neurons, for which we could not observe phenotypic changes upon HERV-K(HML-2) activation (Figures 1H, 1I, and S1M). Indeed,

Please cite this article in press as: Padmanabhan Nair et al., Activation of HERV-K(HML-2) disrupts cortical patterning and neuronal differentiation by increasing NTRK3, Cell Stem Cell (2021), https://doi.org/10.1016/j.stem.2021.04.009

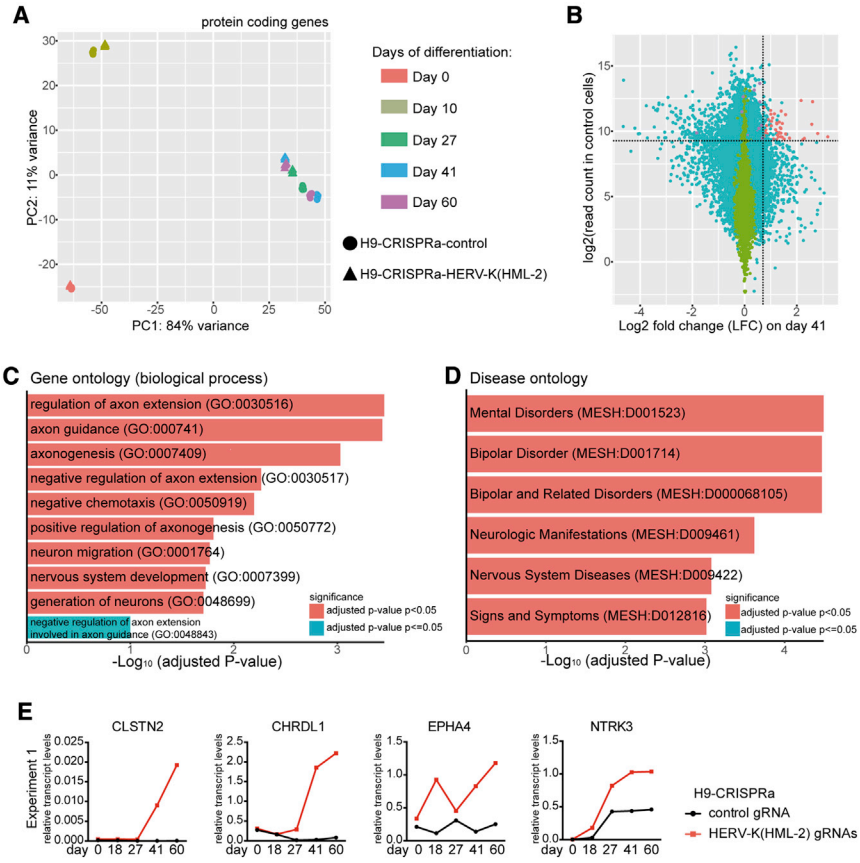

Figure 6. HERV-K(HML-2) overexpression increases expression of neuro-related genes in cortical neurons

(A) RNA-seq data were analyzed for gene expression, and protein-coding genes were visualized by PCA.

(B) Identification of the 28 most significantly upregulated genes in HERV-K(HML-2) activated cells compared to control cells. Each dot depicts a protein-coding gene. Genes above the horizontal dotted line represent the top 25% genes with the highest read count. Genes on the right side of the vertical dotted line are the top 25% upregulated genes on day 41. Blue and green colors correspond to genes with significant differential expression on day 41. Purple color corresponds to genes with read counts among the top 25% and that are among the top 25% upregulated genes on day 60. Red dots depict genes with read counts among the top 25% that are also among the top 25% upregulated genes on days 41 and 60.

(C) Gene Ontology enrichment analysis was carried out to cluster identified genes into biological processes.

(D) Disease enrichment analysis was done to associate the identified genes with diseases.

(E) Expression levels of selected candidates was analyzed by qRT-PCR during the course of cortical neuron differentiation. One biological replicate is shown (see Figure S6 for two more biological replicates).

dopaminergic neurons showed very low *NTRK3* expression in control cell lines that did not increase upon HERV-K(HML-2) activation at day 50 of differentiation (Figure S7D). In contrast, *NTRK3* transcript levels were upregulated at day 60 in cortical neurons, and an even higher increase (2- to 3-fold) was observed when HERV-K(HML-2) was activated (Figure S7D). To further demonstrate that the observed phenotype is caused by increased expression of *NTRK3* upon HERV-K(HML-2) activation, we knocked down *NTRK3* expression in the background of HERV-K(HML-2) activated H9 cells and differentiated the cells into cortical neurons. We observed an ~70% *NTRK3* knockdown efficiency in HERV-K(HML-2) activated cells at the pluripotent stage compared to HERV-K(HML-2) activated cells expressing a non-silencing small hairpin RNA (shRNA) or cells expressing a control gRNA along with a non-silencing shRNA (Figure S7E). At day 35 of cortical differentiation, HERV-K(HML-2) activated cells expressing a non-silencing shRNA showed increased *NTRK3* expression compared to control-gRNA-expressing cells, whereas *NTRK3* expression could be reduced to physiological levels in cells expressing shNTRK3 and HERV-K(HML-2) activated cells (Figure S7E). Importantly, HERV-K(HML-2) activation did not change upon shNTRK3 expression at days 0 and 35 (Figure S7F). Intriguingly, knockdown of *NTRK3* in HERV-K(HML-2) activated cortical neurons completely reverted the reduced neuronal phenotype, resulting in increased *MAP2* levels (Figures 7E and 7F). Moreover, rescue of the morphological phenotype was detected, as illustrated by an increase in neurite length (Figure 7G) and number of segments and extremities (Figure S7G). Notably, the reverted phenotype upon *NTRK3* repression in HERV-K(HML-2) activated cortical neurons is comparable to control cells without HERV-K(HML-2) activation (Figures 7E–7G and S7G). Together, these data propose a model in which HERV-K(HML-2) robustly upregulates *NTRK3*, resulting in aberrant neuronal differentiation and thereby affecting neurite outgrowth (Figure 7H). Importantly, only the knockdown of *NTRK3* in HERV-K(HML-2) activated cortical neurons reverts the observed phenotype (Figure 7H).

DISCUSSION

Our study demonstrates that activation of a specific HERV group, namely HERV-K(HML-2), impedes cortical neuronal differentiation and function and impairs growth and organization of forebrain tissue. We are able to pinpoint the effect of aberrant differentiation driven by HERV-K(HML-2) to one specific gene, namely *NTRK3*, that is upregulated by HERV-K(HML-2) transcriptional activation and, by its own, resembles the phenotype observed upon HERV-K(HML-2) activation.

HERVs have already been associated with neurological disorders (Tam et al., 2019). Although discussed controversially (Garson et al., 2019a, 2019b; Mayer et al., 2018; Prudencio et al., 2017), it has been reported that HERV-K(HML-2) envelope protein (Env) contributes to the development of ALS (Li et al., 2015). Interestingly, even a mild 2-fold overexpression of HERV-K(HML-2) Env in neurons results in ALS neurotoxicity (Li et al., 2015), implicating that fine regulation is needed to maintain

Please cite this article in press as: Padmanabhan Nair et al., Activation of HERV-K(HML-2) disrupts cortical patterning and neuronal differentiation by increasing NTRK3, Cell Stem Cell (2021), https://doi.org/10.1016/j.stem.2021.04.009

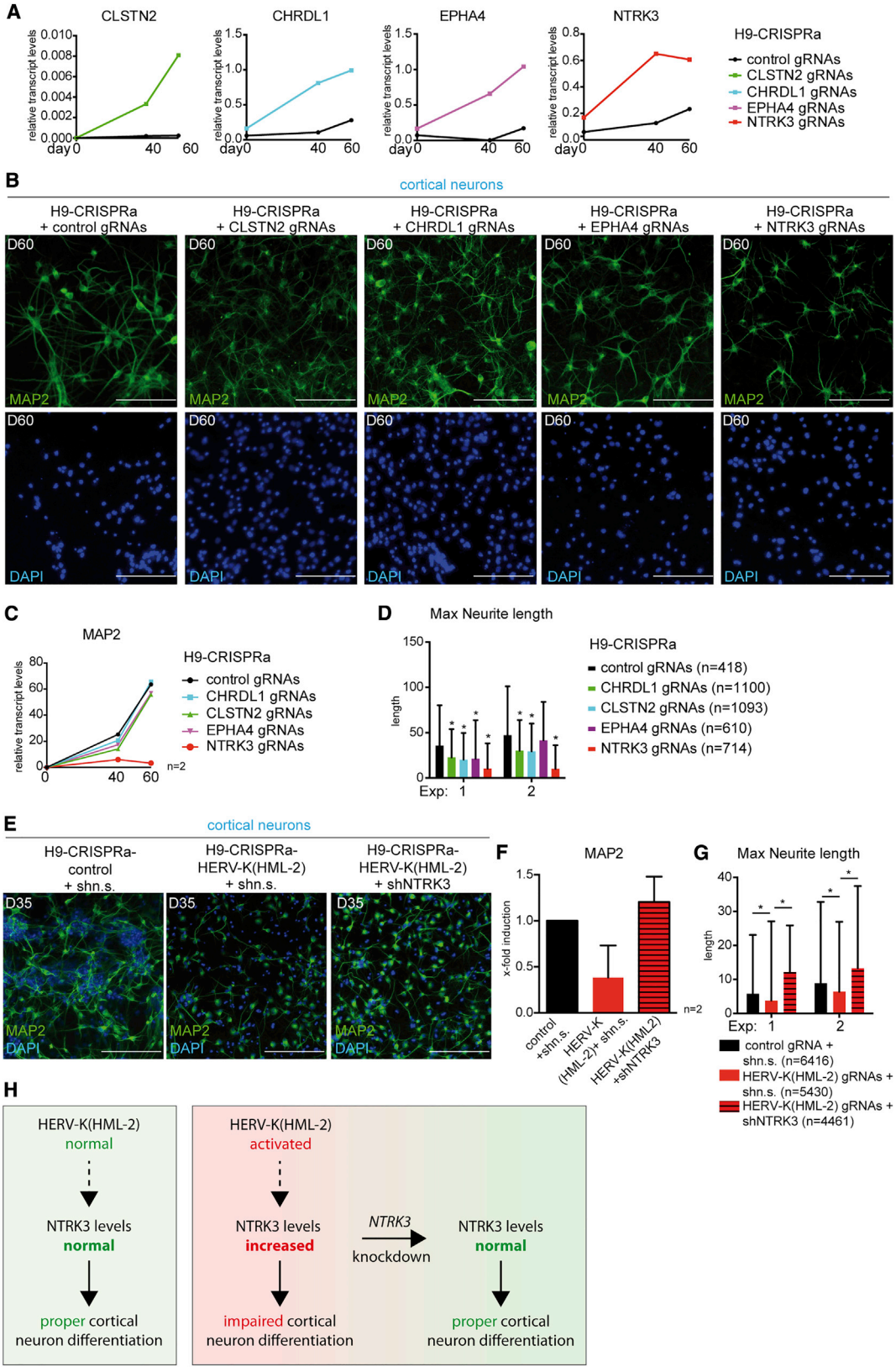

(legend on next page)

Please cite this article in press as: Padmanabhan Nair et al., Activation of HERV-K(HML-2) disrupts cortical patterning and neuronal differentiation by increasing NTRK3, Cell Stem Cell (2021), https://doi.org/10.1016/j.stem.2021.04.009

the healthy state. Recently, it has been reported that downregulation of HERV-K(HML-2) Env promotes neural stem cell differentiation (Wang et al., 2020). Other recent studies showed that a region within HERV-K(HML-2) *env* RNA drives neurotoxicity via Toll-like receptor signaling (Dembny et al., 2020), and repression of HERV-K(HML-2) in neurons decreases interferon-sensitive gene transcripts (Turelli et al., 2020). Also, deletion of KAP1 in mice neurons results in increased ERV expression and inflammatory response (Jönsson et al., 2021). Notably, we did not observe changes in the expression of the HERV-K(HML-2) envelope gene in the course of HERV-K(HML-2) activation (data not shown). In general, the mechanism and regulatory networks controlled by HERV LTRs during the course of neurogenesis and their contribution to the development of neuronal lineages remain elusive.

In this study, we applied CRISPRa and CRISPR inhibition systems to specifically manipulate HERV-K(HML-2) LTRs in hESCs, followed by differentiation into neuronal subtypes, in order to understand their functional role during neuronal development. Activation of HERV-K(HML-2) LTRs, using two different combinations of gRNAs, resulted in lower MAP2 and synapsin I expression as well as a reduced functionality of cortical neurons. Forebrain organoids from HERV-K(HML-2) activated cells were affected in size and displayed less discrete layers of $CTIP2^+$, $TBR1^+$, and $TBR2^+$ cells as well as an absence of $SATB2^+$ neurons. Although we observe a reduction in $CTIP2^+$, $TBR1^+$, and $SATB2^+$ cells upon HERV-K(HML-2) activation using flow cytometry analysis, overall differences in cell numbers were not drastic. Our results suggest that observed changes in forebrain organoids are primarily due to changes in the localization (cytoarchitecture) of specific neurons upon HERV-K(HML-2) activation. The absence of $SATB2^+$ cells in HERV-K(HML-2) activated forebrain organoids could be due to premature differentiation of the precursor cell compartment into deep layer neurons, which would result in smaller organoids. Indeed, we observed a decrease in organoids size upon HERV-K(HML-2) activation (Figure 3B). Furthermore, the changes in CTIP2 and TBR1 expression might be due to loss of SATB2 in HERV-K(HML-2) activated cells, as changes in TBR1 and CTIP2 expression have been linked previously to SATB2 deletion in mice (Britanova et al., 2008). We further detected shorter basal RG cell processes in HERV-K(HML-2) activated organoids (Figure 4G). These defects in the formation of polarized RG progenitors upon HERV-K(HML-2) activation may trigger alterations in RG-guided neuronal migration and neuronal layer formation.

Using RNA-seq, we identified 28 genes as specifically upregulated in HERV-K(HML-2) activated cells during cortical differentiation. The majority of these genes are implicated in neurogenesis and various neurological disorders (Figures 6C, 6D, and S6B). In agreement with those data, we report impaired neurogenesis upon HERV-K(HML-2) activation (Figures 1, 2, 3, 4,and 5). Importantly, we did not detect toxic effects upon HERV-K(HML-2) activation in either cortical neurons or forebrain organoids (Figures 1E, S1L, and S3B–S3D). Thus, we hypothesize that HERV-K(HML-2) activation results in a (too early) (over)expression of these genes, thereby impairing cortical neuronal differentiation. NTRK3, also known as tropomyosin receptor kinase C (TrkC), is an important factor during neuronal development (Bartkowska et al., 2007; Nikoletopoulou et al., 2010; Szobota et al., 2019). NTRK3 binds neurotrophin-3 (NT-3), thereby activating a signaling cascade important for development of cortical precursors and cortical neurons (Bartkowska et al., 2007; McAllister, 2002). Previous work reported that inhibition of NTRK3 (TrkC) signaling results in reduced cortical precursor cell proliferation as well as less migration of neurons into the intermediate zone and cortical plate (Bartkowska et al., 2007). Our results show that upregulation of NTRK3 by HERV-K(HML-2), followed by differentiation into cortical neurons, generates neurons with reduced MAP2 expression and changes in neuronal morphology and neurite outgrowth. Intriguingly, compared to cortical neurons, dopaminergic neurons showed very low levels of NTRK3 expression (Figure S7D), and consequently, their differentiation is not negatively impacted by HERV-K(HML-2) activation (Figure 1H). It has already been shown that neurons of the cerebral cortex express several Trk receptors and neurotrophins throughout each layer (McAllister, 2002; Merlio et al., 1992; Snider, 1994). Interestingly, brain-derived neurotropic factor (BDNF) and NT-3 were described as having opposing effects in regulating neurite outgrowth (McAllister et al., 1997). Therefore, the orchestrated expression of neurotrophins and their receptors during cortical development in both time and space is critical to direct neurite growth and to drive development of neurons and neural circuits.

The transcriptional start site of *NTRK3* is ~283 kb distant from an LTR5_Hs element, an evolutionary young HERV-K(HML-2) LTR. LTR5_Hs has been shown to have the potential to directly

Figure 7. Activation of neurotrophic tyrosine receptor kinase 3 (NTRK3) results in reduced MAP2 expression and changes in neuronal morphology

(A) Activation of selected candidate genes during cortical differentiation was analyzed by qRT-PCR. n = 2 biological replicates.

(B) MAP2 expression was analyzed by immunofluorescence upon selected candidate gene activation. One representative biological replicate is shown. Scale bars, 100 μm.

(C) MAP2 mRNA levels were quantified by qRT-PCR in neurons with CLSTN2, CHRDL1, EPHA4, or NTRK3 transcription activated. n = 2 biological replicates. One representative experiment is shown.

(D) Morphological analysis of cortical neurons upon activation of selected candidate genes. Two biological replicates were quantified.

(E) MAP2 expression was analyzed by immunofluorescence in HERV-K(HML-2) activated cortical neurons expressing shNTRK3 or non-silencing shRNA. One representative biological replicate is shown. Scale bars, 100 μm.

(F) MAP2 levels were quantified using qRT-PCR. The control was set to one and the other conditions were referred to it. Values represent x-fold induction ± SD; n = 2 biological replicates.

(G) Morphological analysis of cortical neurons upon HERV-K(HML-2) activation and knockdown of *NTRK3* expression by shNTRK3. Two biological replicates were quantified.

(H) Model of how HERV-K(HML-2) activation might affect cortical neuron development.

(D–G) Values represent mean ± SD; multiple t test using the Holm-Sidak method (*$p < 0.05$).

affect host gene transcription over long genomic distances of up to ~200 kb upstream or downstream (Fuentes et al., 2018). The identified LTR5_Hs locus is in antisense orientation with regard to *NTRK3*. Therefore, it would need to serve as an antisense promoter to drive *NTRK3* transcription. Notably, several HERV LTRs, particularly HERV-K loci, can serve as antisense promoters (Agoni et al., 2013; Domansky et al., 2000; Manghera et al., 2017). Hence, the phenotype identified upon HERV-K(HML-2) activation in cortical neurons might result from direct activation of *NTRK3* by HERV-K(HML-2). However, it is also possible that the particular LTR5_Hs serves as an enhancer, as it has also been shown that LTR5_Hs elements can impact the activity of genes over longer gene-LTR5_Hs distances (2–245 kb) and independent of its orientation (Fuentes et al., 2018). While we currently cannot specify whether *NTRK3* expression is directly or indirectly regulated by the identified proximal LTR5_Hs element, our findings clearly demonstrate that activation of a specific HERV group, namely HERV-K(HML-2), can impact expression levels of a classical developmental factor, NTRK3, resulting in impaired cortical neuron development and disorganized forebrain organoid patterns. The lack of NTRK3 transcriptional induction in dopaminergic neurons led to normal differentiation even in the presence of HERV-K(HML-2) activation, further strengthening a mechanistic link between the HERV-K(HML-2) LTR5_Hs element and NTRK3.

Typically, expression of HERVs is highly repressed by epigenetic restriction factors such as KAP1 in pluripotent stem cells as well as NPCs (Brattås et al., 2017; Fasching et al., 2015; Jönsson et al., 2021). A recent publication describes that KRAB-zinc-finger proteins facilitate repression of HERVs in a cell-type-specific manner and that repression of HERV-K in neurons decreases interferon-sensitive gene transcripts (Turelli et al., 2020). Thus, future studies will be needed to provide more detailed insights into epigenetic restriction factors contributing to HERV repression across different neural cell types. Although HERVs are typically repressed, they can be reactivated by environmental conditions, including radiation, chemicals, infectious agents (Dolei, 2018; Frank et al., 2006; Hohenadl et al., 1999; Küry et al., 2018), or exogenous viruses (Ruprecht et al., 2006; Tai et al., 2009; Vincendeau et al., 2015). An alternated chromatin state can result in de-silencing and activation of retrotransposons during normal aging (Benayoun et al., 2019; De Cecco et al., 2019; Simon et al., 2019). Intriguingly, many of these HERV reactivation conditions are associated with neurodegenerative diseases (Küry et al., 2018; Tam et al., 2019). In this study, we show that 25 out of 28 identified genes are associated with biological processes implicated in neurodegenerative disease, such as Parkinson's, Alzheimer's, Huntington's, multiple sclerosis, or ALS (Figure S6B). Although further studies will be needed to address the full impact of HERVs on neurological disorders, our study identifies increased NTRK3 expression as a mechanistic link between transcriptional activation of HERV-K(HML-2) and the resulting impairment in cortical development and forebrain organization (Figure 7H). In support of this model, *NTRK3* knockdown in HERV-K(HML-2) activated cells fully rescued this phenotype (Figure 7H). Thus, a tight control of HERV-K(HML-2) expression during cortical differentiation is critical to facilitate the orderly generation of cortical neurons.

Limitations of study

Knowledge of HERV-K(HML-2) proviral and solitary LTR loci becoming transcribed following CRISPRa treatment would be helpful. However, the RNA-seq data (PE100) generated in the course of the study, primarily for gene expression analyses, appear less suited for profiling HERV-K(HML-2) transcriptional activation comprehensively and reliably because of overall high sequence similarities among biologically relevant younger HERV-K(HML-2) loci (Bhardwaj et al., 2015; Montesion et al., 2017; Sexton and Han, 2019; Tatkiewicz et al., 2020). Accordingly, future studies should include RNA-seq experiments using longer read lengths, ideally combined with enrichment of HERV-K(HML-2)-derived transcripts prior to RNA-seq (Tatkiewicz et al., 2020), to yield a further optimized dataset for the detection of HERV-K(HML-2) modulated loci.

STAR★METHODS

Detailed methods are provided in the online version of this paper and include the following:

- KEY RESOURCES TABLE
- RESOURCE AVAILABILITY
  - Lead contact
  - Materials availability
  - Data and code availability
- EXPERIMENTAL MODEL AND SUBJECT DETAILS
  - Cell lines
- METHOD DETAILS
  - Single guide RNA design and cloning
  - Cloning of gRNAs
  - Generation of CRISPRa/i cell lines
  - Generation of gRNA expressing CRISPRa/I cell lines
  - Genomic DNA isolation and PCR amplification
  - Coating plates for differentiation
  - Coating plates for replating with PO/Lam/FN
  - Differentiation into cortical neurons and midbrain dopaminergic neurons
  - Generation of forebrain organoids
  - Immunostaining
  - RNA isolation and reverse transcription
  - Quantitative real-time PCR
  - RNA sequencing and data analysis
  - Differential expression analysis
  - Gene function and network analysis
  - Calcium imaging of cortical neurons
  - Image analysis
  - Quantification of image analysis of organoid sections
  - Flow cytometry analysis
  - Treatment with cell death inhibitors
  - NTRK3 knockdown
- QUANTIFICATION AND STATISTICAL ANALYSIS

SUPPLEMENTAL INFORMATION

Supplemental information can be found online at https://doi.org/10.1016/j.stem.2021.04.009.

ACKNOWLEDGMENTS

We thank Ruth Brack-Werner, Ulrike Protzer, and Maria-Elena Torres-Padilla for extensive discussions, suggestions, and continuous support. Library preparation and RNA-seq were performed at the RNA-seq Core Facility (Institute of Human Genetics, Helmholtz Zentrum München). This work was partly funded by the Deutsche Forschungs Gemeinschaft (DFG, Germany) (fellowship 282609876 to M.V.) and the National Institute of Health (NIH, USA) (grant R01AG054720 to L.S. and core grant P30CA008748). G.C. was supported by an EMBO long-term postdoctoral fellowship (ALTF 311-2015) from the European Molecular Biology Organization and a New York State Stem Cell Science (NYSTEM, USA) postdoctoral fellowship (C32559GG).

AUTHOR CONTRIBUTIONS

M.V. conceived and initiated the project. M.V., L.S., and K.H. designed the study; M.V. and V.P.N. planned the experiments and conducted most experimental work with the support of L.K.; H.L., D.F., G.F., and A.R. performed and interpreted computational data; G.C. helped to interpret cortical differentiations; G.Y.C. and R.W. helped to interpret forebrain organoids data; J.J. and V.N. performed dopaminergic differentiations; J.T. helped to perform calcium imaging; J.M. analyzed HERV-K(HML-2) LTRs, aided in gRNA design, and commented on data; I.R., K.S., and K.H. analyzed and interpreted high-content analysis; and G.C., G.Y.C., T.W.K., and D.C. advised with differentiation protocols. M.V., V.N., and D.F drafted the manuscript; K.H., V.N., D.F., H.L., L.S., J.M., and M.V. edited the manuscript; M.V. finalized the manuscript; and all authors approved the manuscript before submission.

DECLARATION OF INTERESTS

L.S. is a scientific founder and paid consultant of BlueRock Therapeutics and an inventor on patents owned by MSKCC related to the differentiation of dopaminergic and cortical neurons from pluripotent stem cells. The remaining authors declare no competing interests.

Received: July 13, 2020
Revised: March 5, 2021
Accepted: April 12, 2021
Published: May 4, 2021; corrected online: May 18, 2021

REFERENCES

Agoni, L., Guha, C., and Lenz, J. (2013). Detection of Human Endogenous Retrovirus K (HERV-K) Transcripts in Human Prostate Cancer Cell Lines. Front. Oncol. *3*, 180.

Bannert, N., and Kurth, R. (2004). Retroelements and the human genome: new perspectives on an old relation. Proc. Natl. Acad. Sci. USA *101* (*Suppl 2*), 14572–14579.

Bartkowska, K., Paquin, A., Gauthier, A.S., Kaplan, D.R., and Miller, F.D. (2007). Trk signaling regulates neural precursor cell proliferation and differentiation during cortical development. Development *134*, 4369–4380.

Benayoun, B.A., Pollina, E.A., Singh, P.P., Mahmoudi, S., Harel, I., Casey, K.M., Dulken, B.W., Kundaje, A., and Brunet, A. (2019). Remodeling of epigenome and transcriptome landscapes with aging in mice reveals widespread induction of inflammatory responses. Genome Res. *29*, 697–709.

Bhardwaj, N., Montesion, M., Roy, F., and Coffin, J.M. (2015). Differential expression of HERV-K (HML-2) proviruses in cells and virions of the teratocarcinoma cell line Tera-1. Viruses *7*, 939–968.

Brattås, P.L., Jönsson, M.E., Fasching, L., Nelander Wahlestedt, J., Shahsavani, M., Falk, R., Falk, A., Jern, P., Parmar, M., and Jakobsson, J. (2017). TRIM28 Controls a Gene Regulatory Network Based on Endogenous Retroviruses in Human Neural Progenitor Cells. Cell Rep. *18*, 1–11.

Britanova, O., de Juan Romero, C., Cheung, A., Kwan, K.Y., Schwark, M., Gyorgy, A., Vogel, T., Akopov, S., Mitkovski, M., Agoston, D., et al. (2008). Satb2 is a postmitotic determinant for upper-layer neuron specification in the neocortex. Neuron *57*, 378–392.

Buchsbaum, I.Y., Kielkowski, P., Giorgio, G., O'Neill, A.C., Di Giaimo, R., Kyrousi, C., Khattak, S., Sieber, S.A., Robertson, S.P., and Cappello, S. (2020). ECE2 regulates neurogenesis and neuronal migration during human cortical development. EMBO Rep. *21*, e48204.

Buzdin, A., Kovalskaya-Alexandrova, E., Gogvadze, E., and Sverdlov, E. (2006). GREM, a technique for genome-wide isolation and quantitative analysis of promoter active repeats. Nucleic Acids Res. *34*, e67.

Cederquist, G.Y., Asciolla, J.J., Tchieu, J., Walsh, R.M., Cornacchia, D., Resh, M.D., and Studer, L. (2019). Specification of positional identity in forebrain organoids. Nat. Biotechnol. *37*, 436–444.

Chambers, S.M., Fasano, C.A., Papapetrou, E.P., Tomishima, M., Sadelain, M., and Studer, L. (2009). Highly efficient neural conversion of human ES and iPS cells by dual inhibition of SMAD signaling. Nat. Biotechnol. *27*, 275–280.

Chan, S.M., Sapir, T., Park, S.S., Rual, J.F., Contreras-Galindo, R., Reiner, O., and Markovitz, D.M. (2019). The HERV-K accessory protein Np9 controls viability and migration of teratocarcinoma cells. PLoS ONE *14*, e0212970.

Chen, S., Zhou, Y., Chen, Y., and Gu, J. (2018). fastp: an ultra-fast all-in-one FASTQ preprocessor. Bioinformatics *34*, i884–i890.

Chuong, E.B., Elde, N.C., and Feschotte, C. (2016). Regulatory evolution of innate immunity through co-option of endogenous retroviruses. Science *351*, 1083–1087.

Davis, A.P., King, B.L., Mockus, S., Murphy, C.G., Saraceni-Richards, C., Rosenstein, M., Wiegers, T., and Mattingly, C.J. (2011). The Comparative Toxicogenomics Database: update 2011. Nucleic Acids Res. *39*, D1067–D1072.

De Cecco, M., Ito, T., Petrashen, A.P., Elias, A.E., Skvir, N.J., Criscione, S.W., Caligiana, A., Brocculi, G., Adney, E.M., Boeke, J.D., et al. (2019). L1 drives IFN in senescent cells and promotes age-associated inflammation. Nature *566*, 73–78.

Dembny, P., Newman, A.G., Singh, M., Hinz, M., Szczepek, M., Krüger, C., Adalbert, R., Dzaye, O., Trimbuch, T., Wallach, T., et al. (2020). Human endogenous retrovirus HERV-K(HML-2) RNA causes neurodegeneration through Toll-like receptors. JCI Insight *5*, 131093.

Dobin, A., Davis, C.A., Schlesinger, F., Drenkow, J., Zaleski, C., Jha, S., Batut, P., Chaisson, M., and Gingeras, T.R. (2013). STAR: ultrafast universal RNA-seq aligner. Bioinformatics *29*, 15–21.

Dolei, A. (2018). The aliens inside us: HERV-W endogenous retroviruses and multiple sclerosis. Mult. Scler. *24*, 42–47.

Domansky, A.N., Kopantzev, E.P., Snezhkov, E.V., Lebedev, Y.B., Leib-Mosch, C., and Sverdlov, E.D. (2000). Solitary HERV-K LTRs possess bi-directional promoter activity and contain a negative regulatory element in the U5 region. FEBS Lett. *472*, 191–195.

Ecco, G., Cassano, M., Kauzlaric, A., Duc, J., Coluccio, A., Offner, S., Imbeault, M., Rowe, H.M., Turelli, P., and Trono, D. (2016). Transposable Elements and Their KRAB-ZFP Controllers Regulate Gene Expression in Adult Tissues. Dev. Cell *36*, 611–623.

Ellinghaus, D., Kurtz, S., and Willhoeft, U. (2008). LTRharvest, an efficient and flexible software for de novo detection of LTR retrotransposons. BMC Bioinformatics *9*, 18.

Fasching, L., Kapopoulou, A., Sachdeva, R., Petri, R., Jönsson, M.E., Männe, C., Turelli, P., Jern, P., Cammas, F., Trono, D., and Jakobsson, J. (2015). TRIM28 represses transcription of endogenous retroviruses in neural progenitor cells. Cell Rep. *10*, 20–28.

Faulkner, G.J., Kimura, Y., Daub, C.O., Wani, S., Plessy, C., Irvine, K.M., Schroder, K., Cloonan, N., Steptoe, A.L., Lassmann, T., et al. (2009). The regulated retrotransposon transcriptome of mammalian cells. Nat. Genet. *41*, 563–571.

Frank, O., Giehl, M., Zheng, C., Hehlmann, R., Leib-Mösch, C., and Seifarth, W. (2005). Human endogenous retrovirus expression profiles in samples from brains of patients with schizophrenia and bipolar disorders. J. Virol. *79*, 10890–10901.

Frank, O., Jones-Brando, L., Leib-Mosch, C., Yolken, R., and Seifarth, W. (2006). Altered transcriptional activity of human endogenous retroviruses in

neuroepithelial cells after infection with Toxoplasma gondii. J. Infect. Dis. *194*, 1447–1449.

Fuentes, D.R., Swigut, T., and Wysocka, J. (2018). Systematic perturbation of retroviral LTRs reveals widespread long-range effects on human gene regulation. eLife *7*, e35989.

Garson, J.A., Usher, L., Al-Chalabi, A., Huggett, J., Day, E.F., and McCormick, A.L. (2019a). Quantitative analysis of human endogenous retrovirus-K transcripts in postmortem premotor cortex fails to confirm elevated expression of HERV-K RNA in amyotrophic lateral sclerosis. Acta Neuropathol. Commun. *7*, 45.

Garson, J.A., Usher, L., Al-Chalabi, A., Huggett, J., Day, E.F., and McCormick, A.L. (2019b). Response to the Letter from Garcia-Montojo and colleagues concerning our paper entitled, Quantitative analysis of human endogenous retrovirus-K transcripts in postmortem premotor cortex fails to confirm elevated expression of HERV-K RNA in amyotrophic lateral sclerosis. Acta Neuropathol. Commun. *7*, 102.

Guffanti, G., Bartlett, A., DeCrescenzo, P., Macciardi, F., and Hunter, R. (2019). Transposable Elements. Curr. Top. Behav. Neurosci. *42*, 221–246.

Hancks, D.C., and Kazazian, H.H., Jr. (2010). SVA retrotransposons: Evolution and genetic instability. Semin. Cancer Biol. *20*, 234–245.

Harrow, J., Frankish, A., Gonzalez, J.M., Tapanari, E., Diekhans, M., Kokocinski, F., Aken, B.L., Barrell, D., Zadissa, A., Searle, S., et al. (2012). GENCODE: the reference human genome annotation for The ENCODE Project. Genome Res. *22*, 1760–1774.

Helleboid, P.Y., Heusel, M., Duc, J., Piot, C., Thorball, C.W., Coluccio, A., Pontis, J., Imbeault, M., Turelli, P., Aebersold, R., and Trono, D. (2019). The interactome of KRAB zinc finger proteins reveals the evolutionary history of their functional diversification. EMBO J. *38*, e101220.

Hohenadl, C., Germaier, H., Walchner, M., Hagenhofer, M., Herrmann, M., Stürzl, M., Kind, P., Hehlmann, R., Erfle, V., and Leib-Mösch, C. (1999). Transcriptional activation of endogenous retroviral sequences in human epidermal keratinocytes by UVB irradiation. J. Invest. Dermatol. *113*, 587–594.

Jakobsson, J., Cordero, M.I., Bisaz, R., Groner, A.C., Busskamp, V., Bensadoun, J.C., Cammas, F., Losson, R., Mansuy, I.M., Sandi, C., and Trono, D. (2008). KAP1-mediated epigenetic repression in the forebrain modulates behavioral vulnerability to stress. Neuron *60*, 818–831.

Jönsson, M.E., Garza, R., Sharma, Y., Petri, R., Södersten, E., Johansson, J.G., Johansson, P.A., Atacho, D.A., Pircs, K., Madsen, S., et al. (2021). Activation of endogenous retroviruses during brain development causes an inflammatory response. EMBO J. Published online March 1, 2021. https://doi.org/10.15252/embj.2020106423.

Kearns, N.A., Genga, R.M., Enuameh, M.S., Garber, M., Wolfe, S.A., and Maehr, R. (2014). Cas9 effector-mediated regulation of transcription and differentiation in human pluripotent stem cells. Development *141*, 219–223.

Kim, T.W., Piao, J., Koo, S.Y., Kriks, S., Chung, S.Y., Betel, D., Socci, N.D., Choi, S.J., Zabierowski, S., Dubose, B.N., et al. (2021). Biphasic Activation of WNT Signaling Facilitates the Derivation of Midbrain Dopamine Neurons from hESCs for Translational Use. Cell Stem Cell *28*, 343–355.e5.

Kleinstiver, B.P., Prew, M.S., Tsai, S.Q., Topkar, V.V., Nguyen, N.T., Zheng, Z., Gonzales, A.P., Li, Z., Peterson, R.T., Yeh, J.R., et al. (2015). Engineered CRISPR-Cas9 nucleases with altered PAM specificities. Nature *523*, 481–485.

Kriks, S., Shim, J.W., Piao, J., Ganat, Y.M., Wakeman, D.R., Xie, Z., Carrillo-Reid, L., Auyeung, G., Antonacci, C., Buch, A., et al. (2011). Dopamine neurons derived from human ES cells efficiently engraft in animal models of Parkinson's disease. Nature *480*, 547–551.

Kuleshov, M.V., Diaz, J.E.L., Flamholz, Z.N., Keenan, A.B., Lachmann, A., Wojciechowicz, M.L., Cagan, R.L., and Ma'ayan, A. (2019). modEnrichr: a suite of gene set enrichment analysis tools for model organisms. Nucleic Acids Res. *47* (W1), W183–W190.

Küry, P., Nath, A., Créange, A., Dolei, A., Marche, P., Gold, J., Giovannoni, G., Hartung, H.P., and Perron, H. (2018). Human Endogenous Retroviruses in Neurological Diseases. Trends Mol. Med. *24*, 379–394.

Lechner, M., Höhn, V., Brauner, B., Dunger, I., Fobo, G., Frishman, G., Montrone, C., Kastenmüller, G., Waegele, B., and Ruepp, A. (2012). CIDeR: multifactorial interaction networks in human diseases. Genome Biol. *13*, R62.

Li, W., Lee, M.H., Henderson, L., Tyagi, R., Bachani, M., Steiner, J., Campanac, E., Hoffman, D.A., von Geldern, G., Johnson, K., et al. (2015). Human endogenous retrovirus-K contributes to motor neuron disease. Sci. Transl. Med. *7*, 307ra153.

Liao, Y., Smyth, G.K., and Shi, W. (2014). featureCounts: an efficient general purpose program for assigning sequence reads to genomic features. Bioinformatics *30*, 923–930.

Livak, K.J., and Schmittgen, T.D. (2001). Analysis of relative gene expression data using real-time quantitative PCR and the 2(-Delta Delta C(T)) Method. Methods *25*, 402–408.

Love, M.I., Huber, W., and Anders, S. (2014). Moderated estimation of fold change and dispersion for RNA-seq data with DESeq2. Genome Biol. *15*, 550.

Mager, D.L., and Medstrand, P. (2003). Retroviral repeat sequences. In Nature encyclopedia of the human genome, D. Cooper, ed. (Nature Publishing Group).

Manghera, M., Magnusson, A., and Douville, R.N. (2017). The sense behind retroviral anti-sense transcription. Virol. J. *14*, 9.

Maroof, A.M., Keros, S., Tyson, J.A., Ying, S.W., Ganat, Y.M., Merkle, F.T., Liu, B., Goulburn, A., Stanley, E.G., Elefanty, A.G., et al. (2013). Directed differentiation and functional maturation of cortical interneurons from human embryonic stem cells. Cell Stem Cell *12*, 559–572.

Mayer, J., Harz, C., Sanchez, L., Pereira, G.C., Maldener, E., Heras, S.R., Ostrow, L.W., Ravits, J., Batra, R., Meese, E., et al. (2018). Transcriptional profiling of HERV-K(HML-2) in amyotrophic lateral sclerosis and potential implications for expression of HML-2 proteins. Mol. Neurodegener. *13*, 39.

McAllister, A.K. (2002). Neurotrophins and cortical development. Results Probl. Cell Differ. *39*, 89–112.

McAllister, A.K., Katz, L.C., and Lo, D.C. (1997). Opposing roles for endogenous BDNF and NT-3 in regulating cortical dendritic growth. Neuron *18*, 767–778.

Merlio, J.P., Ernfors, P., Jaber, M., and Persson, H. (1992). Molecular cloning of rat trkC and distribution of cells expressing messenger RNAs for members of the trk family in the rat central nervous system. Neuroscience *51*, 513–532.

Montesion, M., Bhardwaj, N., Williams, Z.H., Kuperwasser, C., and Coffin, J.M. (2017). Mechanisms of HERV-K (HML-2) Transcription during Human Mammary Epithelial Cell Transformation. J. Virol. *92*, e01258-17.

Nikoletopoulou, V., Lickert, H., Frade, J.M., Rencurel, C., Giallonardo, P., Zhang, L., Bibel, M., and Barde, Y.A. (2010). Neurotrophin receptors TrkA and TrkC cause neuronal death whereas TrkB does not. Nature *467*, 59–63.

Ovejero, T., Sadones, O., Sánchez-Fito, T., Almenar-Pérez, E., Espejo, J.A., Martín-Martínez, E., Nathanson, L., and Oltra, E. (2020). Activation of Transposable Elements in Immune Cells of Fibromyalgia Patients. Int. J. Mol. Sci. *21*, E1366.

Prudencio, M., Gonzales, P.K., Cook, C.N., Gendron, T.F., Daughrity, L.M., Song, Y., Ebbert, M.T.W., van Blitterswijk, M., Zhang, Y.J., Jansen-West, K., et al. (2017). Repetitive element transcripts are elevated in the brain of C9orf72 ALS/FTLD patients. Hum. Mol. Genet. *26*, 3421–3431.

Prudhomme, S., Oriol, G., and Mallet, F. (2004). A retroviral promoter and a cellular enhancer define a bipartite element which controls env ERVWE1 placental expression. J. Virol. *78*, 12157–12168.

Qi, Y., Zhang, X.J., Renier, N., Wu, Z., Atkin, T., Sun, Z., Ozair, M.Z., Tchieu, J., Zimmer, B., Fattahi, F., et al. (2017). Combined small-molecule inhibition accelerates the derivation of functional cortical neurons from human pluripotent stem cells. Nat. Biotechnol. *35*, 154–163.

Riessland, M., Kolisnyk, B., Kim, T.W., Cheng, J., Ni, J., Pearson, J.A., Park, E.J., Dam, K., Acehan, D., Ramos-Espiritu, L.S., et al. (2019). Loss of SATB1 Induces p21-Dependent Cellular Senescence in Post-mitotic Dopaminergic Neurons. Cell Stem Cell *25*, 514–530.e8.

Ruprecht, K., Obojes, K., Wengel, V., Gronen, F., Kim, K.S., Perron, H., Schneider-Schaulies, J., and Rieckmann, P. (2006). Regulation of human

endogenous retrovirus W protein expression by herpes simplex virus type 1: implications for multiple sclerosis. J. Neurovirol. *12*, 65–71.

Schmitt, K., Richter, C., Backes, C., Meese, E., Ruprecht, K., and Mayer, J. (2013). Comprehensive analysis of human endogenous retrovirus group HERV-W locus transcription in multiple sclerosis brain lesions by high-throughput amplicon sequencing. J. Virol. *87*, 13837–13852.

Seifarth, W., Frank, O., Zeilfelder, U., Spiess, B., Greenwood, A.D., Hehlmann, R., and Leib-Mösch, C. (2005). Comprehensive analysis of human endogenous retrovirus transcriptional activity in human tissues with a retrovirus-specific microarray. J. Virol. *79*, 341–352.

Sexton, C.E., and Han, M.V. (2019). Paired-end mappability of transposable elements in the human genome. Mob. DNA *10*, 29.

Simon, M., Van Meter, M., Ablaeva, J., Ke, Z., Gonzalez, R.S., Taguchi, T., De Cecco, M., Leonova, K.I., Kogan, V., Helfand, S.L., et al. (2019). LINE1 Derepression in Aged Wild-Type and SIRT6-Deficient Mice Drives Inflammation. Cell Metab. *29*, 871–885.e5.

Snider, W.D. (1994). Functions of the neurotrophins during nervous system development: what the knockouts are teaching us. Cell *77*, 627–638.

Szobota, S., Mathur, P.D., Siegel, S., Black, K., Saragovi, H.U., and Foster, A.C. (2019). BDNF, NT-3 and Trk receptor agonist monoclonal antibodies promote neuron survival, neurite extension, and synapse restoration in rat cochlea ex vivo models relevant for hidden hearing loss. PLoS ONE *14*, e0224022.

Tai, A.K., Luka, J., Ablashi, D., and Huber, B.T. (2009). HHV-6A infection induces expression of HERV-K18-encoded superantigen. J. Clin. Virol. *46*, 47–48.

Tam, O.H., Ostrow, L.W., and Gale Hammell, M. (2019). Diseases of the nERVous system: retrotransposon activity in neurodegenerative disease. Mob. DNA *10*, 32.

Tang, L., Yang, F., He, X., Xie, H., Liu, X., Fu, J., Xi, H., Lu, X., Liu, C., Song, Z., et al. (2019). Efficient cleavage resolves PAM preferences of CRISPR-Cas in human cells. Cell Regen. (Lond.) *8*, 44–50.

Tatkiewicz, W., Dickie, J., Bedford, F., Jones, A., Atkin, M., Kiernan, M., Maze, E.A., Agit, B., and Farnham, G. (2020). Characterising a human endogenous retrovirus(HERV)-derived tumour-associated antigen: enriched RNA-Seq analysis of HERV-K(HML-2) in mantle cell lymphoma cell lines. Mob. DNA *11*, 9.

Tchieu, J., Calder, E.L., Guttikonda, S.R., Gutzwiller, E.M., Aromolaran, K.A., Steinbeck, J.A., Goldstein, P.A., and Studer, L. (2019). NFIA is a gliogenic switch enabling rapid derivation of functional human astrocytes from pluripotent stem cells. Nat. Biotechnol. *37*, 267–275.

The Gene Ontology Consortium (2019). The Gene Ontology Resource: 20 years and still GOing strong. Nucleic Acids Res. *47* (D1), D330–D338.

Turelli, P., Playfoot, C., Grun, D., Raclot, C., Pontis, J., Coudray, A., Thorball, C., Duc, J., Pankevich, E.V., Deplancke, B., et al. (2020). Primate-restricted KRAB zinc finger proteins and target retrotransposons control gene expression in human neurons. Sci. Adv. *6*, eaba3200.

van de Lagemaat, L.N., Landry, J.R., Mager, D.L., and Medstrand, P. (2003). Transposable elements in mammals promote regulatory variation and diversification of genes with specialized functions. Trends Genet. *19*, 530–536.

Vincendeau, M., Göttesdorfer, I., Schreml, J.M., Wetie, A.G., Mayer, J., Greenwood, A.D., Helfer, M., Kramer, S., Seifarth, W., Hadian, K., et al. (2015). Modulation of human endogenous retrovirus (HERV) transcription during persistent and de novo HIV-1 infection. Retrovirology *12*, 27.

Wang, J., Xie, G., Singh, M., Ghanbarian, A.T., Raskó, T., Szvetnik, A., Cai, H., Besser, D., Prigione, A., Fuchs, N.V., et al. (2014). Primate-specific endogenous retrovirus-driven transcription defines naive-like stem cells. Nature *516*, 405–409.

Wang, T., Medynets, M., Johnson, K.R., Doucet-O'Hare, T.T., DiSanza, B., Li, W., Xu, Y., Bagnell, A., Tyagi, R., Sampson, K., et al. (2020). Regulation of stem cell function and neuronal differentiation by HERV-K via mTOR pathway. Proc. Natl. Acad. Sci. USA *117*, 17842–17853.

Watanabe, M., Buth, J.E., Vishlaghi, N., de la Torre-Ubieta, L., Taxidis, J., Khakh, B.S., Coppola, G., Pearson, C.A., Yamauchi, K., Gong, D., et al. (2017). Self-Organized Cerebral Organoids with Human-Specific Features Predict Effective Drugs to Combat Zika Virus Infection. Cell Rep. *21*, 517–532.

Zhang, Y., Li, T., Preissl, S., Amaral, M.L., Grinstein, J.D., Farah, E.N., Destici, E., Qiu, Y., Hu, R., Lee, A.Y., et al. (2019). Transcriptionally active HERV-H retrotransposons demarcate topologically associating domains in human pluripotent stem cells. Nat. Genet. *51*, 1380–1388.

Zhou, T., Tan, L., Cederquist, G.Y., Fan, Y., Hartley, B.J., Mukherjee, S., Tomishima, M., Brennand, K.J., Zhang, Q., Schwartz, R.E., et al. (2017). High-Content Screening in hPSC-Neural Progenitors Identifies Drug Candidates that Inhibit Zika Virus Infection in Fetal-like Organoids and Adult Brain. Cell Stem Cell *21*, 274–283.e5.

Please cite this article in press as: Padmanabhan Nair et al., Activation of HERV-K(HML-2) disrupts cortical patterning and neuronal differentiation by increasing NTRK3, Cell Stem Cell (2021), https://doi.org/10.1016/j.stem.2021.04.009

STAR★METHODS

KEY RESOURCES TABLE

REAGENT or RESOURCE	SOURCE	IDENTIFIER
Antibodies		
Mouse monoclonal Anti-CAS9	Abcam	ab191468; RRID:AB_2692325
Mouse monoclonal Anti-GAPDH	EMD Millipore Corp	CB1001-500UG; RRID:AB_2107426
Mouse monoclonal Anti-MAP2	Sigma-Aldrich	M-1406; RRID:AB_477171
Mouse monoclonal Anti-SYNAPSIN-I	SantaCruz Biotech	sc-376623; RRID:AB_11150313
Mouse monoclonal Anti-SOX2	SantaCruz Biotech	sc-365823; RRID:AB_10842165
Rat monoclonal Anti-CTIP2	Abcam	ab18465; RRID:AB_2064130
Mouse monoclonal Anti-OCT-4	SantaCruz Biotech	sc-5279; RRID:AB_628051
Rabbit polyclonal Anti-NANOG	Abcam	ab80892; RRID:AB_2150114
Rabbit polyclonal Anti- PAX6	Biolegend	901301; RRID:AB_2565003
Rabbit polyclonal Anti-TBR1	Abcam	ab31940; RRID:AB_2200219
Rabbit polyclonal Anti-TBR2	EMD Millipore Corp	AB2283; RRID:AB_10806889
Rabbit polyclonal Anti-SATB2	Sigma-Aldrich	HPA001042; RRID:AB_10601711
Mouse monoclonal Anti-Vimentin	Dako	M0725; RRID:AB_10013485
Rabbit monoclonal Caspase 3	Abcam	Ab32351; RRID:AB_725946
Rabbit monoclonal KI67	Invitrogen	MA5-14520; RRID:AB_10979488
AlexaFluor Goat Anti-Mouse 488	Thermo Fischer Scientific	R37120; RRID:AB_2556548
AlexaFluor Goat Anti-Rabbit 488	Thermo Fischer Scientific	A32731; RRID:AB_2633280
AlexaFluor Goat Anti-Rat 488	Abcam	ab150157; RRID:AB_2722511
AlexaFluor Goat Anti-Mouse 594	Abcam	ab150116; RRID:AB_2650601
AlexaFluor Goat Anti-Rabbit 594	Thermo Fischer Scientific	A11012; RRID:AB_141359
AlexaFluor Goat Anti-Rat 568	Thermo Fischer Scientific	A-11077; RRID:AB_141874
AlexaFluor Goat Anti-Rabbit 647	Thermo Fischer Scientific	A-27040; RRID:AB_2536101
Bacterial and virus strains		
E-coli XL10 Gold	Agilent Technologies	200315
E-coli subcloning efficiency DH5α	Thermofischer Scientific	18265017
Chemicals, peptides, and recombinant proteins		
DMEM	Thermo Fischer Scientific	21063-029
Fetal Bovine Serum (FBS)	Thermo Fischer Scientific	10500-064
0.05%Trypsin-EDTA	Thermo Fischer Scientific	25300-054
Knockout Serum (KSR)	Thermo Fischer Scientific	10828010
DMEM-F12 (1:1) Ham	Thermo Fischer Scientific	11320-033
Essential 8 Flex basal media+ E8 Flex supplement (E8 flex)	Thermo Fischer Scientific	A2858501
Essential 6 media (E6)	Thermo Fischer Scientific	A15165-01
Neurobasal media (NB)	Thermo Fischer Scientific	21103-049
L-Glutamine (100X)	Thermo Fischer Scientific	25030-024
N2 supplement (100X)	Thermo Fischer Scientific	17502-048
N2 supplement B (100X)	StemCell Technologies	07156
B27 supplement – Vitamin A (50X)	Thermo Fischer Scientific	12587-010
MEM NEAA	Thermo Fischer Scientific	11140050
Penicillin/Streptomycin (100x)	Thermo Fischer Scientific	15140-122
Sodium Pyruvate (100x)	Thermo Fischer Scientific	11360070
2-mercaptoethanol (1000X)	Thermo Fischer Scientific	21985-023
StemCell Pro Accutase	Thermo Fischer Scientific	A11105-01

(*Continued on next page*)

Please cite this article in press as: Padmanabhan Nair et al., Activation of HERV-K(HML-2) disrupts cortical patterning and neuronal differentiation by increasing NTRK3, Cell Stem Cell (2021), https://doi.org/10.1016/j.stem.2021.04.009

Continued

REAGENT or RESOURCE	SOURCE	IDENTIFIER
Sodium Bicarbonate	Sigma-Aldrich	S5761
0.5M EDTA (pH-8.0), Molecular biology grade	Promega	V4231
Dimethyl Sulfoxide (DMSO)	PanReac Applied Chem	A3672-0250
LDN193189 (LDN)	Stemgent	04-0074
SB431542 (SB)	Tocris	1614
XAV-939 (XAV)	Tocris	3748
Y-27632 dihydrochloride (ROCKi)	Tocris	1254
CHIR99021 (CHIR)	Tocris	4423
DAPT	Tocris	2634
Recombinant Sonic hedgehog (Shh)	R&D biosystems	464-SH-200
Recombinant Brain-derived Neurotrophic Factor (BDNF)	R&D biosystems	248-BD-025
Recombinant Glial-Derived Neurotrophic Factor (GDNF)	PeproTech	450-10
Ascorbic Acid (AA)	Sigma-Aldrich	A4034-100G
db c-AMP	Sigma-Aldrich	D0627-100MG
TGFβ3	R&D Systems	243-B3
Human Insulin	Sigma-Aldrich	I-034
D-(+)-glucose	Sigma-Aldrich	G7021
Progesterone	Sigma-Aldrich	P8783-5G
Mouse Laminin I (LAM)	R&D biosystems	3400-010-1
Human Fibronectin (FN)	EMD Millipore Corp	FC010
Poly-L-Ornithine hydrobromide (PO)	Sigma-Aldrich	P3655
Recombinant Vitronectin (r-VTN)	Thermo Fischer Scientific	A14700
Matrigel	Corning	353234
GelTrex	Thermo Fischer Scientific	A14133-02
Absolute Ethanol (200 proof) molecular biology grade	Fischer Scientific	BP2818-500
Puromycin dihydrochloride cell culture grade	Sigma-Aldrich	P8833
Geneticin G418	Thermo Fischer Scientific	10131027
Polybrene	Sigma-Aldrich	H9268
DAPI	Thermo Fischer Scientific	D1306
O.C.T compound	VWR chemicals	361603E
Richard-Allan Scientific Blue NEG-50	Thermo Fischer Scientific	6502B
Immu-mount	Thermo Fischer Scientific	9990412
Trizol	Thermo Fischer Scientific	15596026
BfuA1	New England Biolabs	R0701S
Critical commercial assays		
RNeasy Mini Kit	QIAGEN	74104
QIAamp DNA mini kit	QIAGEN	51306
Nucleospin Plasmid kit	Macherey-Nagel	740588.50
Nucleobond PC 500 Plasmid Maxi Kit	Macherey-Nagel	740574.25
Nucleospin Gel and PCR clean up	Macherey-Nagel	740609.50
Promega GoTaq Polymerase Kit	Promega	M300
Superscript First strand cDNA synthesis Kit	Thermo Fischer Scientific	11904-018
Agilent RNA 6000 Nano Kit	Agilent Technologies	5067-1511

(*Continued on next page*)

Please cite this article in press as: Padmanabhan Nair et al., Activation of HERV-K(HML-2) disrupts cortical patterning and neuronal differentiation by increasing NTRK3, Cell Stem Cell (2021), https://doi.org/10.1016/j.stem.2021.04.009

Continued

REAGENT or RESOURCE	SOURCE	IDENTIFIER
Deposited data		
RNA seq	This study	GEO: GSE171101
Experimental models: Cell lines		
H9 dCas9-VP64	This study	N/A
H9 dCas9-KRAB	This study	N/A
H9 TRE-dCas9-VP64	This study	N/A
H9 HERV-K dCas9-VP64	This study	N/A
H9 control gRNA dCas9-VP64	This study	N/A
H9 HERV-K dCas9-KRAB	This study	N/A
H9 control gRNA dCas9-KRAB	This study	N/A
H9 HERV-K TRE-dCas9-VP64	This study	N/A
H9 control gRNA TRE-dCas9-VP64	This study	N/A
H9 CHRDL1 dCas9-VP64	This study	N/A
H9 CLSTN2 dCas9-VP64	This study	N/A
H9 EPHA4 dCas9-VP64	This study	N/A
H9 NTRK3 dCas9-VP64	This study	N/A
HEK293T	ATCC	293T/17(HEK293T/17) ATCC®CRL-11268
Oligonucleotides		
gRNAs	This study	provided in Table S2
qRT-PCR Primers	This study	provided in Table S3
Recombinant DNA		
pLKO.1- U6 sgRNA BfuA1 stuffer	Addgene plasmid #50920	A gift from Rene Maehr & Scot Wolfe
pHAGE EFIα dCas9-VP64	Addgene plasmid #50918	A gift from Rene Maehr & Scot Wolfe
pHAGE EFIα dCas9-KRAB	Addgene plasmid #50919	A gift from Rene Maehr & Scot Wolfe
pHAGE TRE-dCas9-VP64	Addgene plasmid #50916	A gift from Rene Maehr & Scot Wolfe
psPAX.2	Addgene plasmid #12260	A gift from Didier Trono
pMD2.G	Addgene plasmid #12259	A gift from Didier Trono
NTRK3 MISSION® shRNA	TRCN0000194821	Sigma-Aldrich
MISSION® pLKO.1-puro Non-Mammalian shRNA Control	SHC002	Sigma-Aldrich
pLKO.1- U6 HERV-K(HML-2) G3	This study	N/A
pLKO.1- U6 HERV-K(HML-2) G10	This study	N/A
pLKO.1- U6 HERV-K(HML-2) G6	This study	N/A
pLKO.1- U6 HERV-K(HML-2) G11	This study	N/A
pLKO.1- U6 CHRDL1 G1	This study	N/A
pLKO.1- U6 CHRDL1 G7	This study	N/A
pLKO.1- U6 CLSTN2 G3	This study	N/A
pLKO.1- U6 CLSTN2 G23	This study	N/A
pLKO.1- U6 EPHA4 G2	This study	N/A
pLKO.1- U6 EPHA4 G11	This study	N/A
pLKO.1- U6 NTRK3 G1	This study	N/A
pLKO.1- U6 NTRK3 G17	This study	N/A
Software and algorithms		
Graph Pad prism 8	GraphPad	https://www.graphpad.com/scientific-software/prism/
ImageJ	NIH	https://imagej.nih.gov/ij/
Adobe Photoshop (CC)	Adobe Inc.	https://www.adobe.com/products/photoshop.html
Adobe Illustrator (CC)	Adobe Inc.	https://www.adobe.com/products/illustrator.html

(*Continued on next page*)

Continued

REAGENT or RESOURCE	SOURCE	IDENTIFIER
Snapgene Viewer	Insightful Science	https://www.snapgene.com:443/
Optimized CRISPR design tool	Zhang Lab, MIT	https://zlab.bio/guide-design-resources
CRISPR-ERA	Lei Stanley Qi Lab, Xiaowo Wang Lab, Stanford	http://crispr-era.stanford.edu
LC480 SW 1.5.1	Roche	https://lifescience.roche.com/en_de/products/lightcycler14301-480-software-version-15.html
Zeiss AX10- Zen Pro 2.3 Blue	Zeiss	https://www.zeiss.com/microscopy/us/products/microscope-software/zen.html
STAR package	Dobin et al., 2013	https://github.com/alexdobin/STAR
GENCODE database version 27	Harrow et al., 2012	https://www.gencodegenes.org/human/release_29.html
featureCounts software	Liao et al., 2014	http://bioinf.wehi.edu.au/featureCounts/
fastp software	Chen et al., 2018	https://github.com/OpenGene/fastp

RESOURCE AVAILABILITY

Lead contact

Further information and requests for reagents should be directed to the Lead Contact, Michelle Vincendeau (michelle.vincendeau@helmholtz-muenchen.de)

Materials availability

Cell lines generated and used in this study are available upon request from the lead contact.

Data and code availability

The accession number for the RNA-seq data reported in this paper is GEO: GSE171101.

EXPERIMENTAL MODEL AND SUBJECT DETAILS

Cell lines

Human pluripotent stem cells (hPSCs) (H9 derivatives (H9-CRISPRa, H9-CRISPRi, H9-CRISPRa-control, H9-CRISPRa-HERV-K(HML-2), H9-CRISPRi-control, H9-CRISPRi-HERV-K(HML-2), H9-TRE-CRISPRa-control, H9-TRE-CRISPRa-HERV-K(HML-2), H9-CRISPRa-CLSTN2, H9-CRISPRa-CHRDL1, H9-CRISPRa-EPHA4 and H9-CRISPRa-NTRK3)) were maintained with Essential 8 Flex media (#A28558501, Thermo Fisher Scientific) in feeder-free conditions on vitronectin (VTN-N) substrate (#A14700, Thermo Fisher Scientific). hPSCs were passaged as clumps with 0.5M EDTA (0.5M EDTA+ 5M NaCl+ 1X PBS). The pluripotency levels of the cells in culture was routinely authenticated for markers Nanog and Oct-4 and checked for mycoplasma contamination.

METHOD DETAILS

Single guide RNA design and cloning

In order to establish CRISPR activation and CRISPR interference cell lines of different HERV groups and selected candidate genes, single guide RNAs were designed using the softwares, Optimized CRISPR design tool (https://www.mit.crispr.edu) or CRISPR-ERA (https://www.crispr-era.stanford.edu). The LTR sequences of different HERV groups or gene sequences of the candidate genes were entered to the web tool and the predicted sgRNA sequences were analyzed for optimal location from transcription start site (TSS) for activation or interference of transcription. A total of two sgRNAs per HERV group or gene were used for experiments. gRNA sequences are listed in Table S2.

Cloning of gRNAs

Lentiviral mammalian expression vector pLKO.1-puro U6 BfuA1stuffer was obtained from addgene (#50902). Guide RNAs were inserted between two BfuA1 sites driven by a U6 promoter. Therefore, gRNAs were annealed at 95°C for 5 minutes and cooled to room temperature o/n. 2μg of the vector was digested using 2 units of BfuA1 enzyme (#R0701S, NEB) at 50°C for 1.5 hours. The enzyme was inactivated at 65°C for 30 minutes. After ensuring complete digestion, the digested vector was purified and 50ng was ligated with 4μL of annealed oligos diluted in 1:100 ratios at 16°C o/n (#M0202S, NEB) following manufacturer's instructions. 5μL of the ligated product was transformed into 30μL of XL10Gold E-coli ultra-competent cells (#200314, Agilent technologies) following the standard

transformation protocol. A control plate containing only vector was included to ensure the efficiency of the cloning protocol. All clones were sent for sequencing and verified for the desired gRNA insertion.

Generation of CRISPRa/i cell lines

pHAGE EF1α dCas9-VP64 lentiviral expression plasmid which encodes a mutated Cas9 fused to a transcription activator VP64 (CRISPRa) (#50918) or transcription repressor KRAB (CRISPRi) (#50919) as well as the plasmid pHAGE TRE dCas9-VP64 (#50919) were a gift from Rene Maehr & Scot Wolfe (Kearns et al., 2014). H9 (WA-09) cells were transduced with lentiviral particles to generate stable H9-dCAS9-VP64 (H9-CRISPRa) or H9-dCAS9-KRAB (H9-CRISPRi) cells, respectively. To this end, Vesicular stomatitis virus G protein pseudotyped lentiviral particles were produced in HEK293T cells. $2x10^6$ cells were seeded in a 10 cm tissue culture dish containing DMEM/F12 (#11320-033, Thermo Fisher Scientific), 10% FCS (#10500-064, Thermo Fisher Scientific) and 1% Pen/Strep (#15140-122, Thermo Fisher Scientific). The next day, cells were transfected using X-treme gene HP DNA transfection reagent (6366244001,Roche) with 1 μg packing plasmid psPAX2(#12260), 1.5 μg VSV-G envelope expressing plasmid pMD2.G(#12259) and 1 μg lentiviral transfer plasmid (pHAGE EF1α dCas9-VP64 or pHAGE EF1α dCas9-KRAB). The cells were stored in 5% CO2 at 37°C for 72h. The supernatant from virus producing HEK293T cells was taken up into a 10 mL syringe and filtered through a Millex HV 0.45 μm falcon filter (#SLHV004SL, Merck Millipore). Cell supernatant containing the virus was concentrated using Amicon Ultra-15 100 kDa ultracentrifugation filter unit (#UFC910024, Merck Millipore) at 2100 rpm for 30 min. The remaining supernatant was taken up into Essential 8Flex basal Medium (#A2858501, GIBCO) to a final volume of 3 mL. Polybrene (#H9268, Sigma-Aldrich) was added to the virus suspension to a concentration of 1 μg/mL. Concentrated virus was used for transduction of H9 cells. Therefore, H9 cells were seeded into Vitronectin (#A14700, Thermo Fisher Scientific) coated 6-well plates. The cells were incubated in 5% CO2 at 37°C with 1ml of the concentrated virus for 24h and then washed with PBS. Transduced cells were selected with 1 μg/μL Puromycin (#P8833, Sigma-Aldrich) in Essential 8 Flex Media (#A28558501, Thermo Fisher Scientific) and maintained for further experiments.

Generation of gRNA expressing CRISPRa/I cell lines

pLKO.1-puro U6 BfuA1stuffer carrying either HERV-K gRNAs, or a CAG control gRNA, or gRNAs directed against the gene of interest were lentivirally transduced into H9-CRISPRa or H9-CRISPRi cells, respectively. Lentiviral production was performed as described previously.

Genomic DNA isolation and PCR amplification

To test for successful lentiviral transduction, genomic DNA of transduced cells was isolated using QIAamp DNA mini kit (#51306, QIAGEN) following manufacturer's instructions. Integration of dCas9 was PCR amplified using specific primers (Table S3) and Promega GoTaq DNA polymerase kit (#M300, Promega) following manufacturer's instructions. 20ng of genomic DNA was used as template. RNA polymerase II (Table S3) was amplified as an internal control. Annealing of primers (dCas9, RPII) were done at 57°C for 30sec.

Coating plates for differentiation

The day before coating thaw Matrigel (#354234, Corning) or Geltrex (#A14133-02, Thermo Fisher Scientific) at 4°C on ice. The next day, dilute Matrigel (1:25) or Geltrex (1:30) with ice cold DMEM/F12 (#11330-032/ Thermo Fisher Scientific) and add Matrigel-DMEM/F12 dilution to the plates (0.5ml/well for 24-well plate or 2ml/well for 6-well plate). Seal the plates with parafilm and store at 4°C o/n.

Coating plates for replating with PO/Lam/FN

Dilute Poly-L-ornithine hydrobromide (PO) (#P3655/Sigma) to 15μg/ml in PBS. Add 0.5ml/well for 24-well plate and incubate over night at 37°C / 5% CO2. Next day, remove the PO solution and wash the plates 3 times with 1X PBS. Afterward dilute Laminin I(3400-010-1,R&D systems) and Fibronectin(FC010, EMD Millipore Corp.) at 2μg/ml in PBS and add 0.5mL/well of a 24-well plate. Incubate the plates at 37°C over night.

Differentiation into cortical neurons and midbrain dopaminergic neurons

The human pluripotent stem cells (hPSCs) (H9 derivatives (H9-CRISPRa, H9-CRISPRi, H9-CRISPRa-control, H9-CRISPRa-HERV-K(HML-2), H9-CRISPRi-control, H9-CRISPRi-HERV-K(HML-2), H9-TRE-CRISPRa-control, H9-TRE-CRISPRa-HERV-K(HML-2) were differentiated into cortical neurons (Maroof et al., 2013; Qi et al., 2017) or midbrain dopamine (mDA) neurons (Chambers et al., 2009; Kriks et al., 2011) following optimized versions of previously published protocols (Kriks et al., 2011; Qi et al., 2017). Briefly, hESCs were dissociated into single cells using Accutase, and plated at high density on Matrigel (#354234, Corning) or Geltrex (#A14133-02, Thermo Fisher Scientific) coated wells. For cortical neuron patterning, cells were cultured in Essential 6 medium (E6, #A1516401, Thermo Fisher Scientific) in the presence of LDN193189 (#72142, Stem Cell Technologies), SB431542 (#1614, Tocris) and XAV939 (#3748, Tocris) (until day 5). From day 5 to 10, cells were cultured in the presence of TGFβ and BMP inhibitors (LDN193189, #72142, Stem Cell Technologies; SB431542, #1614, Tocris) to trigger cortical precursors for cortical neuron differentiation. To induce midbrain floor plate precursors for mDA neuron differentiation cells were culture in the presence of LDN193189 (#72142, Stem Cell Technologies), SB431542 (#1614, Tocris), Sonic hedgehog (#464-SH-200, R&D biosystems) and CHIR99021 (#4423, Tocris) (until day 10). Afterward cells were maintained in mDA differentiation media (Neurobasal media (#21103-049, Thermo

Fisher Scientific), 1% Pen/Strep (#15140-122, Thermo Fisher Scientific), L-Glutamine (#25030-024, Thermo Fisher Scientific), B27-Vitamin A (#12587010, Thermo Fisher Scientific)) supplemented with DAPT (#2634, Tocris), BDNF (#450-10, PreproTech), GDNF (#248-BD-025, R&D biosystems), cAMP (#D0627, Sigma), AA (#4034-100, Sigma) and TGF-β3 (#243-B3, R&D biosystems) as described previously (Kim et al., 2021; Kriks et al., 2011; Qi et al., 2017). For cortical neuron induction, cortical precursors were maintained in mDA differentiation media in the absence of TGFβ3. mDA neurons and cortical neurons were cultured on polyornithine (PO)/laminin (L)/fibronectin (FN) coated wells.

Generation of forebrain organoids

Forebrain organoids were generated from hPSCs following the protocol described in (Zhou et al., 2017). Briefly, hPSCs were dissociated into single cells using Accutase (#A11105-01, Thermo Fisher Scientific) for 30 minutes at 37°C. Afterward, cells were aggregated using low-adhesion V-bottom plates (#MS-9096V, Wako) in Essential 8 Flex media (#A28558501, Thermo Fisher Scientific) with 10 μM ROCK inhibitor (Y-27632, #1254, Tocris) (day-1). At day0, media was changed to Essential 6 medium (E6, #A1516401, Thermo Fisher Scientific) in the presence of 500 nM LDN193189 (#04-0074, Stemgent) and 2mM XAV-939 (#3748, Tocris) until day 4. XAV-939 was removed from day 4 till day 18. Afterward, organoids were maintained in organoid differentiation medium (50% DMEM F-12 (#11320-033, Thermo Fisher Scientific), 50% Neurobasal media (#21103-049, Thermo Fisher Scientific), 0.5xN2 supplement (#17502-048, Thermo Fisher Scientific), 0.025% insulin (#I-034, Sigma), 5 mM L-Glutamine (#25030-024, Thermo Fisher Scientific), 0.7 mM MEM-NEAA (#11140050, Thermo Fisher Scientific), 50 U/mL Penicillin-Streptomycin (#15140-122, Thermo Fisher Scientific), 55 mM 2-mercaptoethanol (#21985-023, Thermo Fisher Scientific), 1xB27 supplement -Vitamin A (#12587010, Thermo Fisher Scientific).

Immunostaining

Human PSCs were washed once with 1X PBS and fixed with 4% PFA for 15 min at room temperature. Cells were permeabilized with 0.03% Triton X-100/PBS for 10 min and washed twice in 0.15% Triton X-100/PBS at room temperature. Blocking was done in 0.15% Triton X-100/PBS supplied with 5% BSA (40mg/mL) for 60 minutes at room temperature. Cells were incubated with primary antibody in 0.15% Triton X-100/PBS supplied with 5% BSA (40mg/mL) o/n at 4°C. Next day, cells were washed three times with 0.15% Triton X-100/PBS and incubated with secondary antibody in 0.15% Triton X-100/PBS supplied with 5% BSA for 2 hours. 90 minutes post incubation, nuclear stain DAPI was added. Finally, cells were washed three times with 0.15% Triton X-100/PBS and imaged using a Zeiss (AX10) microscope.

Organoids were fixed in 4% PFA overnight at 4°C. The next day they were washed three times in PBS. After fixation, organoids were cryoprotected in 30% sucrose/PBS and sectioned at 20μM on a cryostat (Leica 1850 UV). Sections were blocked in 10% FBS, 0,3% Triton X-100/PBS and incubated as floating section in primary antibody overnight. The next day, sections were washed three times with PBS and incubated with secondary antibody for 3 hours at room temperature. Afterward, sections were mounted onto slides and imaged using a Zeiss (AX10) microscope. We used established protocols for staining brain organoids (Cederquist et al., 2019; Watanabe et al., 2017).

RNA isolation and reverse transcription

Total RNA from hPSCs was isolated using TRIzoL (#15596-026, Invitrogen) following manufacturer's protocol. RNA extraction was performed using chloroform. RNA was precipitated in isopropanol and resuspended in nuclease free ddH2O. Total RNA (1μg) was reverse transcribed using Superscript First Strand Synthesis kit following manufacturer's protocol using random hexamers.

Quantitative real-time PCR

QRT-PCR was performed using specific primers (see Table S3) and the LightCycler® 480 SYBR Green I (#04887352001, Roche) on a Roche LightCycler 480 II qPCR system. Relative gene expression was calculated using the −ΔΔCt method (Livak and Schmittgen, 2001). All genes were normalized to RNA polymerase II values. Primer sequences are listed in Table S3.

RNA sequencing and data analysis

For RNaseq the RNA integrity number (RIN) was measured using the Agilent 2100 Bioanalyzer system. RNA with a RIN value higher then 8 were sent for whole genome RNA sequencing. The TruSeq RNA Sample Preparation kit (Illumina) was used synthesizing the cDNA libraries and sequenced in paired-end-reads with the HiSeq4000 sequencer (Illumina) at Helmholtz Zentrum München RNaseq Core Facility. Quality control and preprocessing of RNaseq data was done by fastp (Chen et al., 2018) with default parameters. Pair-end reads were mapped to the human reference genome (assembly GRCh38) using the STAR package with all default parameters (Dobin et al., 2013). We used the comprehensive gene annotation on the primary assembly (chromosomes and scaffolds) sequence regions contained in the GENCODE database version 27 (Harrow et al., 2012). The reads mapped to genes were counted using the feature Counts software (Liao et al., 2014). We only retained read pairs that successfully aligned to the same chromosome (command line options -B, -C, -p set) and discarded multi-mapped read pairs (option -M not specified). Genes with very low read counts (< 10) in all samples were excluded from consideration.

Differential expression analysis

The differential expression (DE) analysis of protein coding genes in the H9-CRISPRa-HERV-K(HML-2) and H9-CRISPRa-control at different time points was effected by the DESeq2 package (Love et al., 2014). The overall differences between samples were

assessed by the Principal Component Analysis (PCA) upon applying the regularized-logarithm transformation to the raw read count data in order to stabilize the variance across the means of the genes. For the differential analysis read counts were modeled by a negative binomial distribution, using a design matrix to identify the cell type associated with each sample. In order to produce more stable estimates for genes with low read count, the level of differential expression was measured by shrunken Log2 fold change (LFC) values. Genes with high adjusted p values (FDR > = 0.1) were discarded. For each gene we determined the maximal mapped read count number measured in the control cell over five time points. For example, if for a certain gene the read counts for control cell on day 0, 10, 27, 41, and 60 were 1572, 1793, 2092, 2183, and 2005, respectively, that gene was represented by the maximum read count number 2183. Subsequently genes were ranked according to the maximal read count number in the control cell and only top 25% of genes were retained for further analysis. We also ranked the LFC values of genes differentially expressed between the HERV-K(HML-2) guide RNA cells and control cells separately for each time. Subsequently we selected those genes whose LFC values were among the top 25% of the LFC values consistently over two time points: D41 and D60. For example, if the upregulated genes with the top 25% of the LFC values were G1, G3, G5, G6, G7 at D41, and G3, G5, G8, G9 at D60, only the genes G3 and G5 would be selected as consistently differentially expressed over these two time points. We selected for experimental verification only those genes that a) exhibited a high read count in the control cells, thus providing sufficient statistical evidence for DE assessment, and b) were significantly upregulated over two continuous time points: day 41 and day 60. Based on the gene and HERV coordinates provided in the human genome annotation and the HERVd database, respectively, we identified the HERV-K(HML-2) LTRs located with a 500 kb vicinity of the transcript start sites (TSS) of these genes.

Gene function and network analysis

Gene Ontology (GO) (The Gene Ontology Consortium, 2019) and Mammalian Phenotype Ontology (MPO) enrichment analysis of the differentially expressed genes was performed using the modEnrichr suite (Kuleshov et al., 2019). Disease enrichment analysis was effected with the help of the Set Analyzer tool provided by the Comparative Toxicogenomics Database (CTD) (Davis et al., 2011). A manually curated gene-disease interaction network for the neurodegenerative diseases was obtained from the CIDeR database (Lechner et al., 2012) and three publicly available text-mining tools: Chilibot, Polysearch2, and Google Scholar.

Calcium imaging of cortical neurons

hPSC-derived neural stem cells were plated onto PO/Lam/FN coated 0.5mm black ΔT dishes (*#10199-774, VWR)* and used for calcium imaging as described (Tchieu et al., 2019). At day 60 of cortical neuronal differentiation, neurons were incubated with 5μM of Fura-2 (#F1221, Thermo Fisher Scientific) for 30 minutes at 37°C. Cultures were perfused with normal Tyrode's solution (pH 7.4) and supplemented with glutamate (100 μM), ATP (30 μM) or KCl (65mM) for 1 minute. Images were taken every 30 s at 340 and 380 nm. Images were analyzed by calculating the signal ratio between 380/340 using FIJI (ImageJ).

Image analysis

Multiparametric image analysis was performed using Columbus high-content imaging and analysis software version 2.8.0 (PerkinElmer Life Sciences). Dapi signal was used to detect cell nuclei using the Method M with the following parameters: common threshold (parameter determining the lower level of pixel intensity for the whole image that may belong to nuclei): 0.2; area (to tune the merging and splitting of nuclei during nuclei detection): > 25 μm; splitting coefficient (parameter influencing the decision of the computer whether a large object is split into two or more smaller objects or not): 0,4. Next, the morphology of nuclei and the Dapi and GFP-signal intensity (MAP2) was calculated and the nuclei were filtered by some of these properties (nucleus length < 100 px and nucleus roundness > 0,87; nucleus area > 100 px). For this subpopulation the building block "CSIRO Neurite Analysis 2" was used. This building block identifies neurites growing from a cell body. The neurite analysis consists of two steps: first Neurite detection and second the neurite tree analysis: the neurites are split into segments, assigned to individual cells and quantified. The analysis tool calculates following parameters: Maximum Neurite length (length of the longest neurite attached to the cell body), Number of Extremities, Number of Roots, Number of Segments, Number of Nodes type 1 and type 2 and the Total Neurite Length. For analysis of SynapsinI expression in the neurite segment population the "find spots"-building block was applied using method C.

Quantification of image analysis of organoid sections

For quantification of image analysis we divided the developing cortex in five equal bins as described in (Buchsbaum et al., 2020); bin1 corresponding to ventricular zone, bin2/bin3 corresponding to SVZ and bin4/bin5 corresponding to cortical plate of the cortex. In each bin either single cells were counted using the manual cell counter of ImageJ or intensities were measured using ImageJ. Cell numbers were set relative to the overall number of positive cells and displayed as percentage of positive cells.

Flow cytometry analysis

At day 60 of organoid generation two organoids were pooled and flow cytometry analysis was performed as described in (Buchsbaum et al., 2020). Briefly, organoids were washed with PBS and dissociated using Accutase. Afterward cells were washed with PBS and centrifuged for 5 min at 300 g. The cell suspension was filtered through a 100μm cell strainer and again centrifuged for 5 min at 300 g. Next, cells were fixed using 70% ice-cold Ethanol for 1h on ice. After fixation cells were centrifuged for 30 min at 300 g (4°C) and washed in staining buffer (1% FCS in PBS). Afterward samples were stained with the corresponding primary antibodies in staining buffer for 30 min on ice, followed by washing with staining buffer and another 30 min of secondary antibody staining

on ice. The labeled cells were then washed with staining buffer and resuspended in PBS for FACS analysis. FACS analysis was performed using a FACS CantoII (BD).

Treatment with cell death inhibitors

Cortical neurons were differentiated as described above, in the presence of either an apoptosis inhibitor (z-VAD-FMK, 20μM), a ferroptosis inhibitor (Ferrostatin-1, 1μM) or a necroptosis inhibitor (Necrostatin-1, 10μM). Inhibitors were added to the corresponding media throughout the differentiation until day60, starting at day0.

NTRK3 knockdown

For knockdown experiments corresponding cells were transduced with the mission shRNA (TRCN0000194821/SHCLNG-NM_002530) or a non-silencing shRNA and differentiated into cortical neurons as described above.

QUANTIFICATION AND STATISTICAL ANALYSIS

At least three independent biological replicates were performed if not otherwise indicated. For organoids three independent biological replicates were performed and three organoids per time point were sectioned and stained. *p* values were calculated by unpaired two-tailed Student's t test if not otherwise specifically indicated (*$p < 0.05$, **$p < 0.01$ and ***$p < 0.001$). Values are presented as mean ± SD.